Titania on silica: a case study for cyclohexene epoxidation toward flow applications

Léa Gonçalves, Michele Scotto Di Perta, Karim Bouchmella, Johan Alauzun, Patrick Cognet, Peter Hesemann, Carine Julcour

▶ **To cite this version:**

Léa Gonçalves, Michele Scotto Di Perta, Karim Bouchmella, Johan Alauzun, Patrick Cognet, et al.. Titania on silica: a case study for cyclohexene epoxidation toward flow applications. Industrial and engineering chemistry research, 2024, 63 (36), pp.15745-15760. 10.1021/acs.iecr.4c01672 . hal-04715631

HAL Id: hal-04715631
https://hal.umontpellier.fr/hal-04715631v1

Submitted on 7 Oct 2024

HAL is a multi-disciplinary open access archive for the deposit and dissemination of scientific research documents, whether they are published or not. The documents may come from teaching and research institutions in France or abroad, or from public or private research centers.

L'archive ouverte pluridisciplinaire **HAL**, est destinée au dépôt et à la diffusion de documents scientifiques de niveau recherche, publiés ou non, émanant des établissements d'enseignement et de recherche français ou étrangers, des laboratoires publics ou privés.

Manuscript prepared as a full paper for submission to
Industrial & Engineering Chemistry Research

Titania on Silica, a case study for cyclohexene epoxidation towards flow applications

Léa Gonçalves[1†], Michele Scotto di Perta[2†], Karim Bouchmella[1], Johan G. Alauzun[1], Patrick Cognet[2], Peter Hesemann[1*], Carine Julcour[2*]

[1] ICGM, Univ Montpellier-CNRS-ENSCM, 1919, route de Mende, 34293 Montpellier Cedex 05, France.

[2] Laboratoire de Génie Chimique, CNRS, INPT, UPS, Université de Toulouse, 4 Allée Emile Monso, Toulouse 31432, France

[†] contributed equally to this manuscript

carine.julcour@toulouse-inp.fr

peter.hesemann@umontpellier.fr

Keywords

Silica, titania, surface grafting, epoxidation, green solvent, kinetic modelling

Graphical Abstract

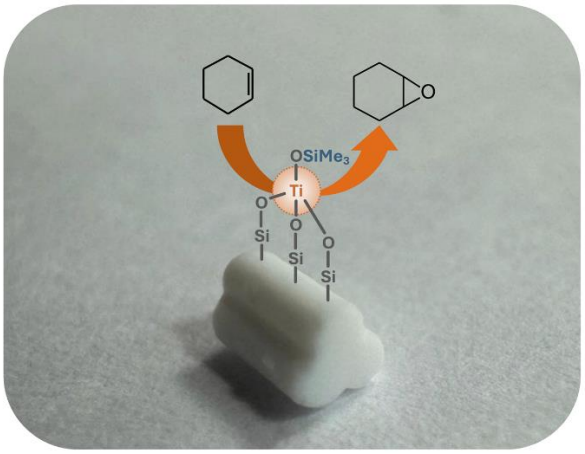

Abstract

We report the synthesis of a titanium-based catalyst supported on silica pellets and its use as heterogeneous catalyst for the epoxidation of cyclohexene. Commercially available SiO_2 trilobe-shaped pellets (NorPro) were modified in a two-step procedure including Ti species grafting followed by surface passivation using hexamethyldisilazane (HMDS). The amount of active metal could be controlled via the variation of the quantity of the titanium precursor. The materials were characterized via EDX, UV-Vis, XPS, and ^{29}Si solid-state NMR. All investigations confirmed the presence of dispersed titanium (IV) species grafted as well on the outer as on the inner surface of the silica pellets, mainly in a tetrahedral environment. The successful passivation via trimethylsilylation was monitored via ^{29}Si solid state NMR spectroscopy. The use of the materials as heterogeneous epoxidation catalyst showed that the amount of immobilized Ti(IV) species has a strong effect on the catalytic properties of the materials. In particular, a material displaying a Si/Ti molar ratio of 33 offered a good compromise between optimized Ti content, catalytic activity/selectivity, and re-usability. A kinetic study of the epoxidation reaction was carried out in an environmentally friendly solvent, cyclopentyl methyl ether. The apparent kinetics were successfully fitted by an Eley-Rideal model describing product inhibition with negligible adsorption of cyclohexene.

1 Introduction

Epoxidation of alkenes is a key industrial reaction, with only ethylene oxide and propylene oxide being produced over 25 Mt in 2008.[1-3] Indeed, these epoxides are most commonly used for the formulation of epoxy glues and plastics.[4, 5] Due to the high reactivity of the oxirane ring, they are also the main intermediates for the synthesis of a variety of fine chemical products, such as ethylene glycol and propylene glycol as antifreeze agents or monomers.[6-8] In addition, epoxidation of higher or cyclic olefins finds applications in the valorization of CO_2,[9, 10] the production of bio-derived products,[11-13] perfumes,[14] pharmaceutical chemicals[15-17] and polymers.[18-21] While the homogeneous dehydrochlorination of chlorohydrins remains a prominent method for propylene oxide synthesis,[3, 22] metal-catalyzed transformations operated in either the homogeneous or the heterogeneous phase[23, 24] have gained ground due to their reduced environmental impact. In this context, heterogeneous approaches are preferred since they facilitate straightforward catalyst separation and recycling. Dispersed transition metal oxides typically composed of Ti, Mo or V immobilized on siliceous supports were found to be active catalysts for epoxidation of alkenes.[25-27] On the other hand, bulk metal oxides such as ZrO_2, Nb_2O_5, and Ta_2O_5 turned to be unselective.[28] Among successful catalysts, titanium silicalite (TS-1), a framework-substituted redox molecular sieve, has gained tremendous interest in the selective oxidation of propene to propylene oxide by hydrogen peroxide.[29, 30] This process, known as HPPO (for "hydrogen peroxide to propylene oxide") and developed separately by Evonik/Uhde and BASF/Dow Chemical, produces only water as a by-product. [31, 32] However, its application to bulkier olefins is limited by their low solubility in the aqueous H_2O_2 phase requiring the use of a suitable (co-)solvent, as well as the narrow size of the zeolite pores (< 1 nm) which precludes their access to the internal active sites.[33, 34] Other technologies avoiding the generation of co-products include the propylene oxide cumene process developed by Sumitomo Chemicals. Here, cumene hydroperoxide is used as an oxidizing agent: the produced cumyl alcohol can indeed be recycled into cumene hydroperoxide by hydrogenation followed by cumene oxidation in air. This process involves a mesoporous Ti-SiO_2 catalyst which has been designed to activate larger molecules and to exhibit high hydrophobicity, thus increasing its affinity for alkenes.[1]

Another challenge associated to the reaction is related to its high exothermicity (with a heat of reaction of -200 to -250 kJ/mol),[35] which most often requires the use of a solvent to mitigate the temperature rise. Methanol, acetonitrile, dichloromethane, and toluene have classically been reported, but the use of greener alternatives is deemed important to increase the process

sustainability. Furthermore, the solvent can influence the formation of the transition state, thereby affecting the reaction performance and selectivity.[33, 36-40]

The aim of this work is to synthesize an active, selective, and stable Ti-based catalyst, supported on a commercial SiO_2 support, for the epoxidation of cyclohexene by cumene hydroperoxide in cyclopentyl methyl ether (CMPE), an eco-friendly solvent.[41, 42] CPME exhibits a relatively high boiling point of 106°C (but significantly lower than that of cyclohexene oxide, 130°C), a low vaporization energy, and high chemical stability which makes it a candidate of choice for applications in catalytic epoxidation reactions. The proposed catalyst is in the form of millimeter-sized pellets, allowing its application in a continuous reactor of fixed bed type, for process scale-up. To this end, an apparent kinetic model is provided and limitation effects by internal diffusion are examined.

2 Experimental section

2.1 Materials and methods

The silica trilobe-shaped carrier (ref. SS69139) was provided by Saint-Gobain NorPro (France). Titanium(IV) isopropoxide $Ti(OiPr)_4$ (97%), hexamethyldisilazane (HMDS, 99%), *n*-decane (99%), cyclohexene (99%), and cumene hydroperoxide (80% in cumene) were purchased from Sigma-Aldrich and Fisher Scientific. Isopropanol (99.7%) and toluene (99.8%), purchased from VWR and Fisher Scientific, respectively, were dried with molecular sieves (rods, Supelco) under argon atmosphere. The molecular sieves were activated at 200°C under reduced pressure and transferred into a Rotaflo flask. The amount of water in the anhydrous solvents was measured by a Karl Fischer titration method with a TitroLine KF trace Titrator instrument (SI Analytics). Toluene and isopropanol showed a water concentration lower than 20 ppm. Cyclopentyl methyl ether (99.9+%) was obtained from Fisher Scientific and used without further purification.

The surface to volume ratio of the trilobes was obtained by image processing of cross-sectional cuts on a Morphologi G3 (Malvern Instruments). Nitrogen adsorption-desorption isotherms on the silica before and after surface modifications were obtained at 77 K using a Micromeritics Tristar II Plus analyzer. The samples were degassed under reduced pressure at 200°C and 40°C, respectively. The specific surface area was calculated using the Brunauer-Emmett-Teller (BET) theory in the 0.05-0.30 P/P_0 range. Total pore volume was measured at $P/P_0 = 0.99$. The mesopore volume and average pore diameter were estimated with the Barrett-Joyner-Halenda

(BJH) method. In addition, the size distribution of mesopores and macropores in the silica support and the Ti-grafted catalyst was measured by mercury intrusion porosimetry on a Micromeritics Autopore IV apparatus, operating with a pressure up to 400 MPa. The structural density of the solids was measured by an AccuPyc II 1345 (Micromeritics) helium pycnometer.

Titanium distribution across the catalytic pellets was probed using a field emission gun-scanning electron microscope (JEOL JSM 7100F FEG-SEM) equipped with an energy-dispersive X-ray spectrometer (Oxford ASDD X-Max EDX detector). Mapping of the catalyst outer surface was also carried out on a Zeiss EVO HD15 microscope equipped with an Oxford Instruments X-Max ^{N} SDD EDX detector. Total titanium content in the selected catalyst was also measured by ICP-AES after acid digestion at Antellis laboratory (Toulouse, France). Finally, the dispersion of the Ti species was examined on a transmission electron microscope equipped with a 200kV field emission gun (JEOL 2200FS – 200 KV FEG-TEM) and with an energy-dispersive X-ray spectrometer (EDX – SDD Oxford Instrument XMaxN 100 TLE detector).

Solid-state Nuclear Magnetic Resonance (NMR) analyses were carried out at the NMR platform of ICGM. ^{29}Si solid-state NMR spectra were recorded on a 300 MHz Varian VNMRS300 (7.05 Tesla Wide Bore magnet), with a Varian T3 MAS (Magic Angle Spinning) probe and 7.5 mm ZrO_2 rotors. Measurements were carried out using the non-quantitative CPMAS technique with ^{1}H decoupling (Cross Polarisation Magic Angle Spinning/magnetization transfer from ^{1}H to ^{29}Si followed by ^{1}H decoupling), with a recycling time of 3 s, a $\pi/2$ pulse of 5 µs and a contact time of 5 ms. The chemical shift was calibrated using a secondary reference of Q8M8H (octakis(dimethylsiloxy)octasilsesquioxane), whose left-hand signal was fixed at -2.25 ppm.

Solid-state diffuse-reflectance UV-vis spectrum of the catalyst was recorded on a CARY 5000 spectrometer on the 190-400 nm wavelength range with a step of 0.5 nm.

X-ray photoelectron emission spectra (XPS) were recorded on a Thermo Scientific K-Alpha spectrometer, using a monochromatic source with an aluminium anode ($h\upsilon$ = 1486.6 eV) and a spot size of 400 µm (CIRIMAT, Toulouse). The calibration energy of the spectrometer was performed using the reference peak C 1s (284.9 ± 0.1 eV). High-resolution scans of C 1s, O 1s, Si 2p, and Ti 2p were acquired with a 30 eV pass energy with an increment value of 0.1 eV.

2.2 Preparation of the heterogeneous epoxidation catalysts

Epoxidation catalysts with various Si/Ti molar ratios were synthesized by surface modification of silica trilobe-shaped supports (SiO_2-tri).[43, 44] SiO_2 pellets were dried and heated at 200°C under reduced pressure for 12 h, then under argon for 6 h. The following steps were performed in anhydrous conditions, using an argon flow. The dried silica trilobes were suspended in anhydrous isopropanol. Then, different amounts of $Ti[O^iPr]_4$ were added to this suspension (*cf.* Table 1~~Table 1~~) depending on the targeted Si/Ti ratio. The suspensions were heated at 130°C without stirring for 22 h. The resulting solids were recovered by filtration, washed with isopropanol, and dried under reduced pressure for 12 h at 200°C. Then, the solids were calcined in a muffle furnace at 600°C for 5 h. These materials were labelled 'TiO_2@SiO_2-tri-np'.

The silica surface was then passivated by trimethylsilanization. The selected amount of passivating agent *vs.* SiO_2 was based on passivation tests carried out with different quantities of hexamethyldisilazane (HMDS), according to a previously published protocol.[45, 46] ^{29}Si solid-state NMR (CPMAS) analyses were used to select the optimal passivation of the support by integrating the contributions of Q^2, Q^3 and Q^4 species. Lower silanol species (Q^2, Q^3) were observed when the molar ratio of the passivating agent *vs.* SiO_2 was 0.3 (see **Figure 4**~~**Figure 6**~~ in section 3.1). The TiO_2@SiO_2-tri-np materials were first heated at 150°C for 1 h under argon and then dried under vacuum at 150°C for 2 h.[46] The solids were then suspended in anhydrous toluene and HMDS was added (HDMS/Si = 0.3). The suspensions were heated at 150°C for 2 h under argon atmosphere. The solids were recovered by filtration and washed three times with 20 mL of toluene, acetone, and ethanol up to a neutral pH of the filtrate. The silanized solids were finally dried under reduced pressure at 40°C for 12 h, thus giving the Ti-grafted and passivated solids 'TiO_2@SiO_2-tri-pX' (X = 1 to 5, with increasing Ti content). In addition, a passivated silica carrier without Ti (SiO_2-tri-p) was prepared according to the abovementioned procedure for comparison.

a mis en
Non Gras
a mis en
Non Gras
a mis en
Non Gras

Table 1. Amounts of precursors used for titanium-grafting and passivation of silica trilobe-shaped pellets and resulting Si/Ti molar ratios

Sample	Mass of Ti[^{i}PrO]$_4$ (g/g of silica pellets)	Volume of HMDS (mL/g of silica pellets)	Si/Ti molar ratio: pellet cross-section (outer surface) [(a)]
SiO_2-tri-p	0	1.0	n/a
TiO_2@SiO_2-tri-p1	0.03	1.0	(153)
TiO_2@SiO_2-tri-p2	0.06	1.0	74 (80)
TiO_2@SiO_2-tri-p3	0.12	1.0	57 (64)
TiO_2@SiO_2-tri-p4	0.35	1.0	33
TiO_2@SiO_2-tri-p5	0.49	1.0	33 (23)

(a) Si/Ti ratios were determined from elemental mapping of pellet cross-sectional cuts (profile lines) and outer surfaces, with a coefficient of variation of 10-15% (5 to 6 pellets) and 4-9% (1 pellet, 3 measures each), respectively.

2.3 Catalytic tests

Preliminary catalytic tests of cyclohexene epoxidation were carried out in a 25 mL double-neck round-bottom flask, equipped with a condenser under argon atmosphere. The catalyst (100 mg) was first dried overnight under reduced pressure at 60°C. The cyclohexene (7 g, 0.084 mol) was added with 2 mL of anhydrous toluene and 1 mL of decane, used as internal standard. The mixture was then heated to 75°C under magnetic stirring (600 rpm) and cumene hydroperoxide (CHP, 4 g, 0.021 mol) was added. Recyclability and stability tests for the catalyst were carried out under identical to those used in the screening tests, only varying the quantities of reactants employed (6.6 g, 0.079 mol of cyclohexene, and 4.3 g, 0.022 mol of CHP). Aliquots of the reactive medium were collected after various reaction times and stored in a freezer. The reaction was monitored by using a gas chromatograph GC-2010 (Shimadzu) coupled with a mass spectrometer GCMS-QP2010 Plus (Shimadzu). The column used was a HP-5 from Agilent (5% phenyl methyl siloxane, 30 m in length and 0.25 mm of internal diameter, with a film thickness of 0.25 μm). The injection temperature was set to 250°C and injections (1 μL) were performed using a split ratio of 40.

Kinetic studies were carried out in a 150 mL glass batch reactor, equipped with a three-blade stirrer, a jacket connected to a thermostatic bath, a condenser, and a fixed annular catalyst basket to avoid particle breaking or attrition. The operating protocol was as follows for the reference

conditions using ca. 2 M concentration of cyclohexene and a stoichiometric amount of oxidant. The catalyst (1 g), solvent (cyclopentyl methyl ether, 31 mL), oxidant (cumene hydroperoxide 80 wt.%, 25 mL, 0.14 mol), and internal standard (octane, 5 mL, 0.03 mol) were introduced into the reactor. The reaction mixture was heated at 80°C and cyclohexene (14 mL, 0.14 mol) was then added to the reactor. The reaction was completed after heating for 6 h under stirring at 600 rpm. Samples were taken at regular time intervals and analyzed immediately or stored in a refrigerator. The reactants and products were quantified using a Trace 1300 gas chromatograph (Thermo Fisher Scientific) equipped with a flame ionization detector (FID). Separation was performed on a TG5-MS column (5% phenyl methyl siloxane, Thermo Scientific) with dimensions of 30 m × 0.25 mm × 25 μm. The injection temperature was set to 200°C, the injection volume to 1 μL and the split ratio to 50. The temperature of the detector was 250°C. The oven was held at the initial temperature of 50°C for 5 minutes and then increased at 10°C/min until it reached 150°C, at which it was held for another 5 minutes. Besides cyclohexene oxide (CHO), 2-cyclohexen-1-ol, 2-cyclohexen-1-one and cyclohexane-1,2-diol were evaluated as possible by-products. The yields of the cyclohexene oxidation products were defined with respect to the initial number of moles of the alkene in the reaction mixture (n_{CH_0}):

$$Y_{j_{(t)}} = \frac{n_{j_{(t)}} - n_{j_0}}{n_{CH_0}} \qquad (1)$$

(where $n_{j(t)}$ and n_{j_0} are the number of moles of the cyclohexene oxidation product j at time t and zero time of the reaction, respectively).

3 Results and discussion

3.1 Surface modification of silica trilobe-shaped pellets and characterization of the materials

The synthesis of the silica-supported epoxidation catalyst was achieved in a two-step sequence starting from silica trilobe-shaped pellets (Saint-Gobain NorPro, France), including (*i*) the surface grafting of titanium species via an impregnation/calcination step, and (*ii*) the passivation of the surface. Trilobe-shaped silica pellets were first reacted with titanium(IV) isopropoxide ($Ti(O^iPr)_4$). Calcination of the Ti-impregnated objects led to the formation of silica pellets containing highly dispersed titanium species. In a second step, the silica surface was passivated by trimethylsilanization of residual hydroxyl groups with hexamethyl disilazane (HMDS) in

order to decrease water adsorption capacity, and therefore increase catalyst selectivity and stability by preventing epoxide ring-opening that results in the formation of diols, and Ti-O-Si hydrolysis.[47]

We then performed the chemical and physico-chemical characterization of the materials. Here, the characteristics of the TiO_2@SiO_2-tri-p4 material are given as a representative example. The material was analyzed by electron microscopy coupled with EDX, nitrogen sorption, mercury porosimetry, X-ray diffraction, XPS and ^{29}Si solid state NMR spectroscopy. These analyses give detailed information about the chemical composition of the material, as well as its morphological and textural characteristics.

3.1.1 Electronic imaging and elemental mapping

Scanning Electron Microscopy (SEM) was used to visualize the morphology and the texture of silica trilobe-shaped carriers, before and after surface modification via Ti-grafting and silanization (**Figure ~~Figure 1~~**). These trilobe-shaped extrudates have an average length of about 3 mm and a lobe diameter of ca. 1 mm.

An average projected area of 2.7±0.1 mm^2 with an external perimeter of 6.7±0.2 mm was estimated by the Morphologi software v8.30 from the analysis of ten cross-sectional cut images recorded with an optical microscope (magnification of 2.5× and particle stitching method). This results in a surface to volume ratio of 3.1 mm^{-1} for the pellets (*i.e.*, a sphere-equivalent diameter of 1.9 mm).

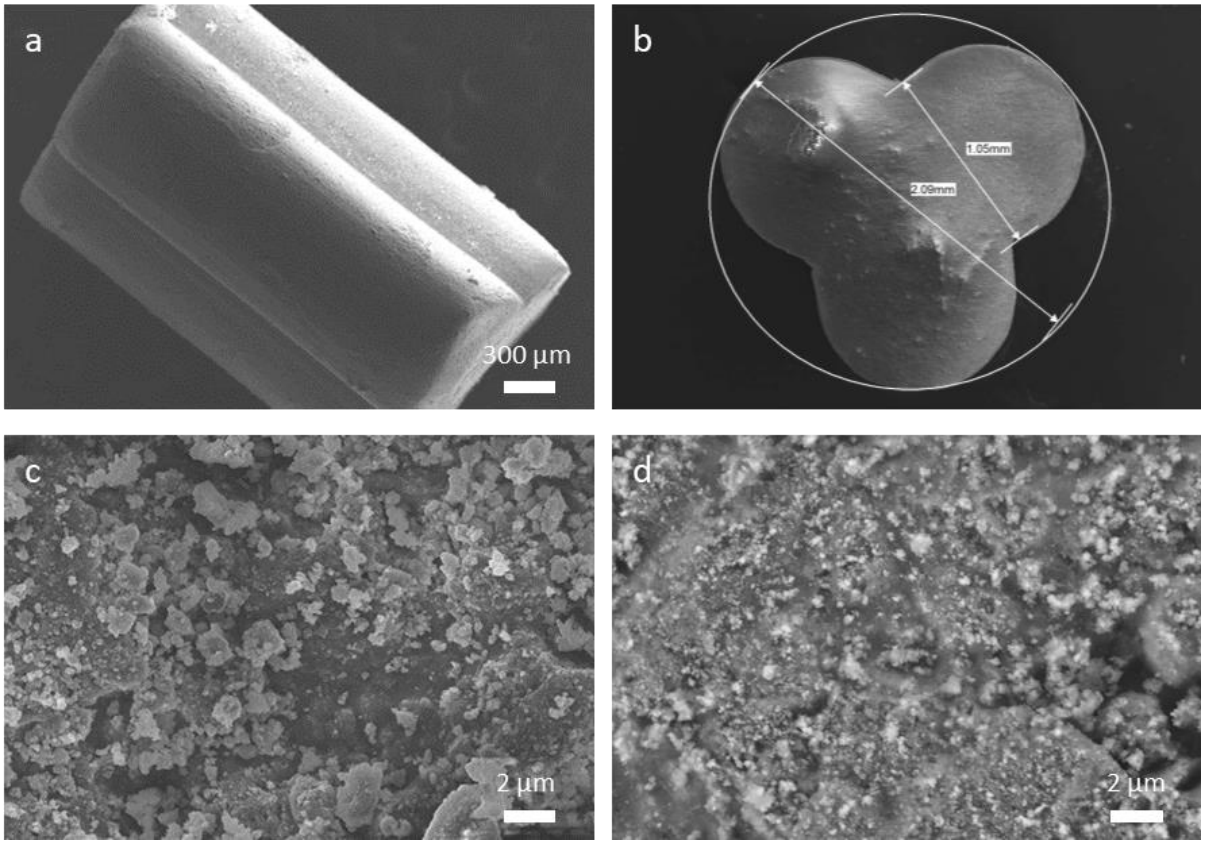

Figure 1. SEM images of the silica trilobe-shaped pellets: (a) and (b) particle morphology, (c) and (d) zoom views on the surface of the silica support and TiO_2@SiO_2-tri-p4, respectively

The surface of the silica support (**Figure ~~Figure 1~~c**) is covered by agglomerated primary particles, resulting in extra-granular porosity, in addition to internal porosity. After titanium grafting and passivation, there was no significant difference in the surface roughness of the material (**Figure ~~Figure 1~~d**).

SEM/EDX mapping was used to determine the elemental composition of the materials and to demonstrate the dispersion of titanium species after the impregnation of the silica supports with titanium(IV) isopropoxide. For the sake of comparability, we determined in particular the Si/Ti ratio of the formed materials. Variation in the titanium content of the materials could indeed be achieved using different amounts of the titanium precursor during the impregnation process. The Si/Ti ratios of the whole series of materials are given in **Table 1~~Table 1~~**. The obtained materials display a Si/Ti molar ratio in the range of 23-153 on their outer surface.

Furthermore, the elemental line profiles carried out on the cross-sections of the catalysts, **Figure ~~Figure 2~~**, show that Ti can be found as well on the outer surface of the particles as on their inner surface. The internal Si/Ti molar ratio is also close to that measured on the surface

(see Table 1~~Table 1~~). Thus, Ti has successfully been grafted onto the whole surface of the pellets. The amount of Ti grafted seems to reach a plateau for the highest concentration of titanium(IV) isopropoxide, since Si/Ti ratios measured inside the pellets are similar for TiO_2@SiO_2-tri-p4 and TiO_2@SiO_2-tri-p5. It corresponds to a Ti content of ca. 2 wt.%, which was confirmed by ICP-AES analysis after acid digestion.

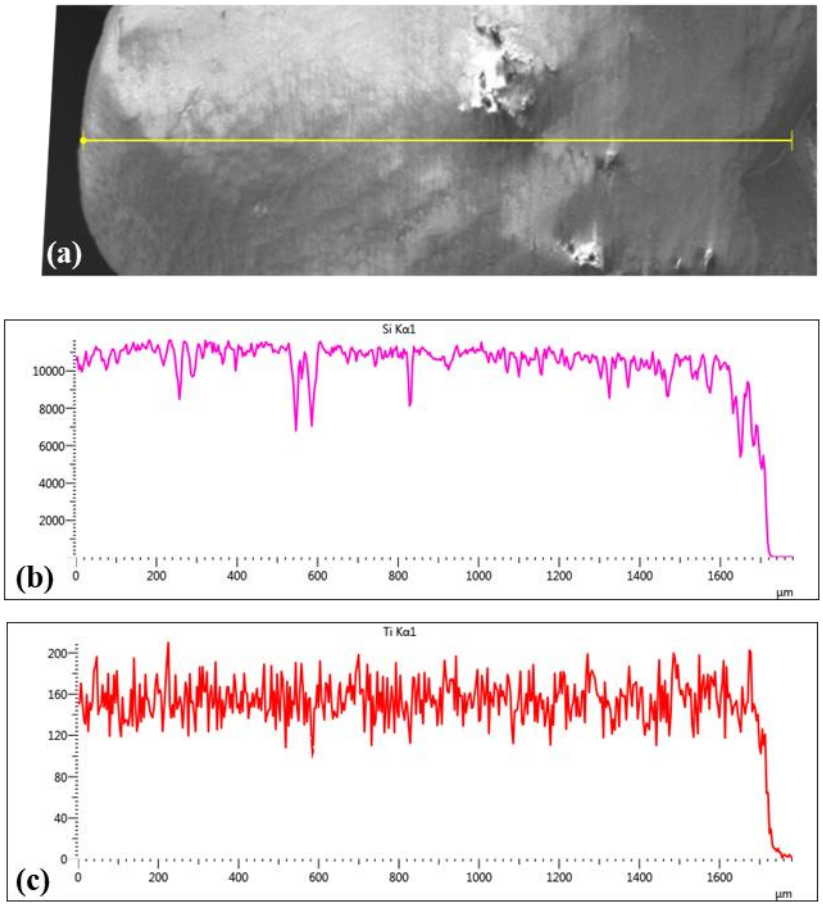

Figure 2. SEM image of the cross-section of the TiO_2@SiO_2-tri-p4 catalyst extrudate (a), along with EDX elemental line profiles of silicon (b) and titanium (c)

In addition, Figure 1~~Figure 3~~ shows the titanium mapping of the surface of TiO_2@SiO_2-tri-p1 from TEM/EDX, indicating that the Ti species are highly dispersed over the whole surface.

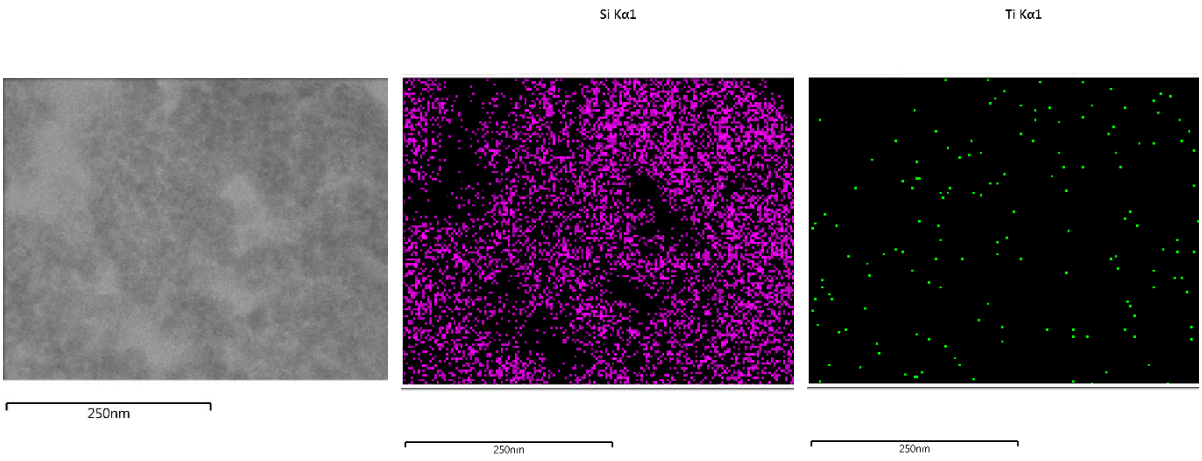

(a) **(b)** **(c)**

Figure 1~~3~~. STEM image of TiO_2@SiO_2-tri-p1 catalyst (a) and corresponding EDX silicon (b) and titanium (c) mapping of the surface

3.1.2 Textural properties

Nitrogen sorption experiments were performed in order to determine the effect of titanium grafting and passivation on the textural characteristics of the material. The nitrogen sorption isotherms of these materials are shown in **Figure 2. ~~Figure 4~~**, and the corresponding specific surface area, pore volume, and pore size are given in

Table 2~~Table 2~~. The sorption isotherms of all the materials display a very similar shape with a type IV isotherm, which is characteristic of mesoporous materials with a narrow size of pores. This behaviour indicates a very similar texture of the three materials. The passivation reaction clearly results in a decrease of specific surface area, pore size and pore volume - from 200 $m^2.g^{-1}$ for the parent material to approx. 170 $m^2.g^{-1}$ after the passivation reaction, whereas the Ti impregnation and calcination affect the texture of the material only to a lesser extent. The distribution of pore width calculated by the BJH method spans between 6 and 20 nm and is centered at around 11 nm for all the samples. The pore size is only slightly affected both by the Ti-grafting and the passivation reaction.

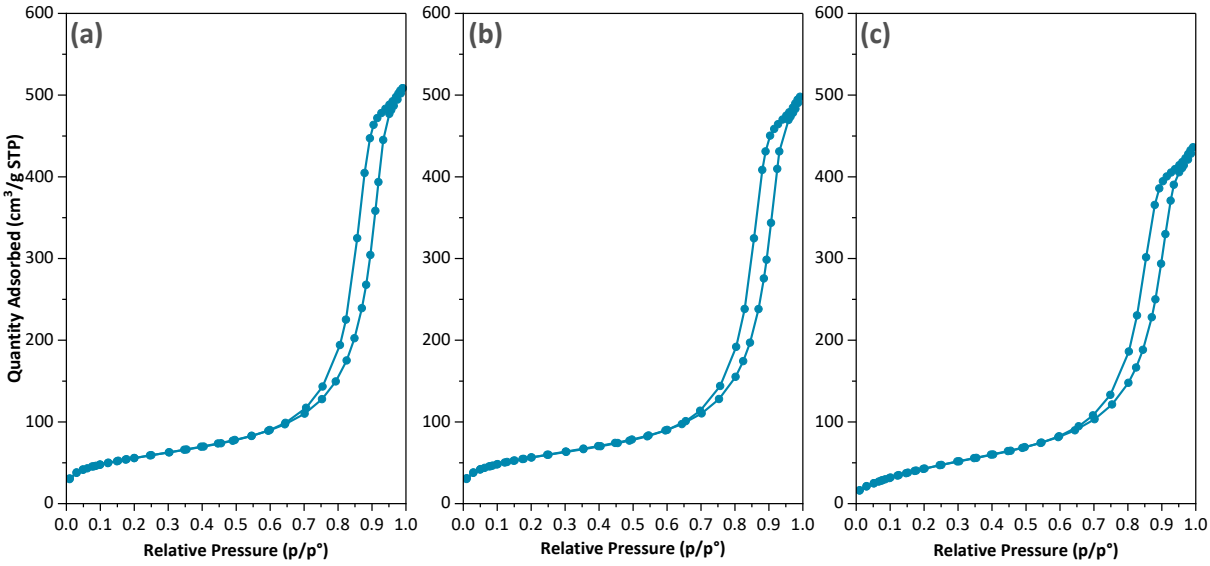

Figure 24. Nitrogen sorption isotherms of (a) native silica pellets, (b) pellets after Ti-grafting (TiO_2@SiO_2-tri-np4), and (c) after passivation (TiO_2@SiO_2-tri-p4)

Table 2. Effect of titanium-grafting and passivation on the specific surface area and pore volume of the silica pellets

Sample	Gas porosimetry				Mercury intrusion	
	BET surface area ($m^2.g^{-1}$) [(a)]	Total pore volume ($cm^3.g^{-1}$) [(b)]	Mesopore volume ($cm^3.g^{-1}$) [(c)]	Average pore width (nm) [(c)]	Mesopore volume ($cm^3.g^{-1}$) [(d)]	Macropore volume ($cm^3.g^{-1}$) [(e)]
SiO_2-tri	199	0.79	0.76	12	0.72	0.15
SiO_2-tri-p	168	0.71	0.69	10	-	-
TiO_2@SiO_2-tri-np4	199	0.77	0.74	12	-	-
TiO_2@SiO_2-tri-p4	172	0.67	0.65	12	0.63	0.14

[(a)] $0.05 < P/P_0 < 0.3$
[(b)] Total pore volume at $P/P_0 = 0.99$
[(c)] From BJH desorption (pore width: 4V/A)
[(d)] Pore size range: 3-45 nm (using Washburn equation)
[(e)] Pore size range: 45-250 nm (using Washburn equation)

In addition to nitrogen sorption, mercury porosimetry and helium pycnometry were performed to determine the mesoporous and macroporous volumes (*cf.*

Table 2~~Table 2~~) and the density of these materials, respectively. Mercury intrusion/extrusion curves (*cf.* **Figure S1**) display a flat plateau at high pressures, indicating a complete pore filling, as well as a hysteresis loop (of type H1), with extrusion occurring at a lower pressure than intrusion. This hysteresis behavior is classically related to the complexity of the pore network

and/or to a shift in the dynamic contact angle between intrusion (advancing) and extrusion (receding) with an impact of surface roughness.[48] Some mercury entrapment in the largest pores is also seen at the first cycle, but the loop closes in the following cycle. The mesoporous volume measured by mercury intrusion is in very good agreement with that obtained from gas porosimetry. Additionally, macropores account for about 20% of the total porosity (*cf.* **Table 2**~~**Table 2**~~). Finally, the structural density of the solids is found to be 2.2 g.cm^{-3}.

3.1.3 X-ray diffraction and spectroscopic analyses

X-ray diffraction (XRD) of the materials was used to investigate the presence of crystalline phases within the materials. XRD patterns of both silica carriers with and without surface modifications (**Figure S2**) show only one broad diffraction peak at 22°,[49, 50] characteristic for amorphous phases. The absence of diffraction peaks suggests the absence of crystallized TiO_2 phases such as anatase or rutile.

The UV-Vis diffuse-reflectance spectrum of the TiO_2@SiO_2-tri-p4 catalyst (**Figure S3**) exhibits a broad band spanning over 190-340 nm with a maximum centered around 220 nm, which can be attributed to isolated $Ti(OSi)_4$ sites, and a slight shoulder around 260 nm possibly due to the presence of a very few Ti oxide oligomers.[51]

X-ray photoelectron spectroscopy (XPS) aimed at gaining insights into the Si and Ti coordination in the catalyst samples. XPS spectra of carbon, oxygen, silicon and titanium of the TiO_2@SiO_2-tri-p4 surface are shown in **Figure 3**~~**Figure 5**~~. They give the binding energy levels of the emitted electrons, and thus information on the chemical environment for each detected element (here C, O, Si, Ti).

C 1s, O 1s, and Si 2p spectra exhibit all single peaks centered at 103, 285, and 533 eV, respectively. The first one can be assigned to carbon atoms originating from $SiMe_3$ groups.[52] The other two correspond to the oxygen and silicon atoms contained in the Si-O-Si bulk groups of silica, respectively.[53, 54] The contribution of silanol groups (at 532 eV on the O 1s spectrum) was not detected, nor that of Ti-O-Ti bond (at 530 eV on the O 1s spectrum). [55, 56]

Two broad signals are observed in the titanium region (Ti 2p). These two contributions, centered at 459 and 465 eV, can be deconvoluted using OriginPro 2022b software into two different peaks each (**Figure 3**~~**Figure 5**~~**d**). The peaks at 464 and 466 eV correspond to photoelectrons emitted from the $2p_{1/2}$ level, while the most intense peaks located at 458 and 460 eV correspond to the Ti $2p_{3/2}$ energy level. For each signal, the highest binding energy

component (centered at 460 and 466 eV, respectively) is assigned to Ti(IV) in a tetrahedral environment, and the lowest ones (458 and 464 eV, respectively) can be attributed to penta- or hexacoordinated titanium centers.[45, 57] The deconvolution gives a surface ratio of 2.6 and 2.9 for 460 *vs*. 458 eV and 466 *vs*. 464 eV, respectively. Thus, with peak areas for the high binding energy component that are about 3 times those of the low binding energy counterpart, XPS results demonstrate the most prominent contribution of the $Ti(OSi)_4$ species which are usually reported to be more active and selective in epoxidation.[47]

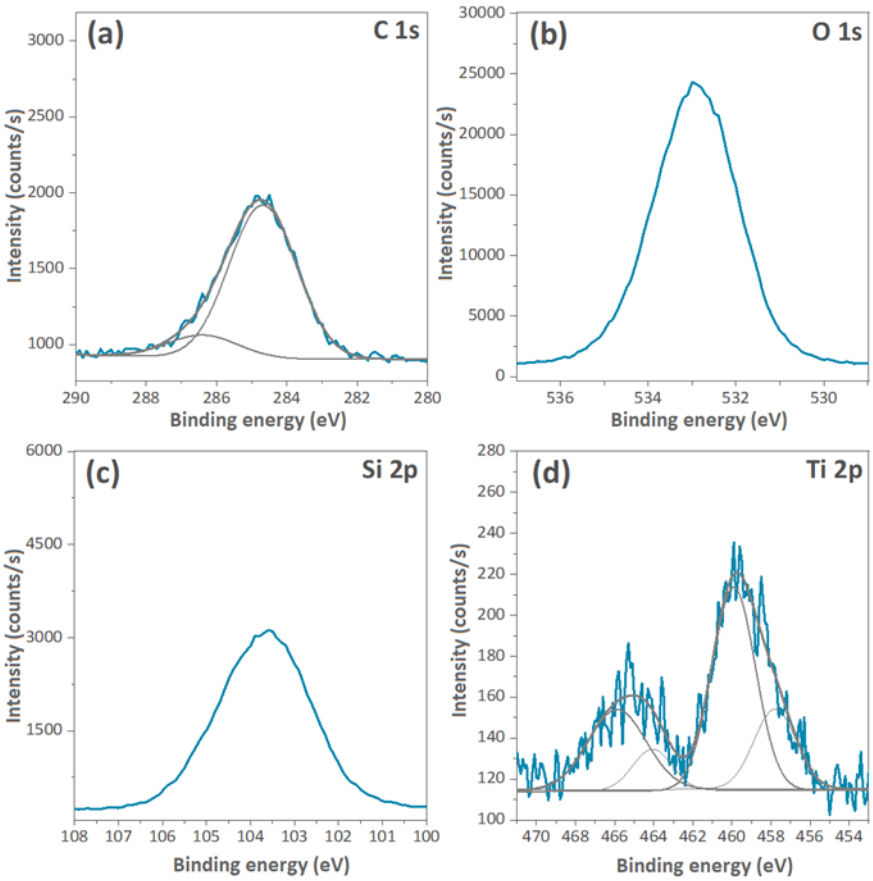

Figure 3~~5~~. XPS spectra of the TiO_2@SiO_2-tri-p4 catalyst: (a) C 1 s, (b) O 1s, (c) Si 2p, and (d) Ti 2p

^{29}Si solid-state NMR was used to study the environment of silicon centers in TiO_2@SiO_2-tri-p4 (**Figure 4~~Figure 6~~**). The spectrum was deconvoluted using the Dmfit program.[58] Two different contributions, centered at 13 and -110 ppm, can be observed on the ^{29}Si spectrum of the TiO_2@SiO_2-tri-p4 material. The first peak can be ascribed to the $SiMe_3$ groups that are introduced via the passivation step. The second signal can be deconvoluted into three peaks located at -90, -100, and -110 ppm and correspond to Q^2, Q^3 and Q^4 silicate units, respectively. Even though no quantification could be performed (CP MAS experiment), the low intensities

of the Q^2 and Q^3 species qualitatively reflect the low residual amount of hydroxyl groups after the trimethylsilanization step.

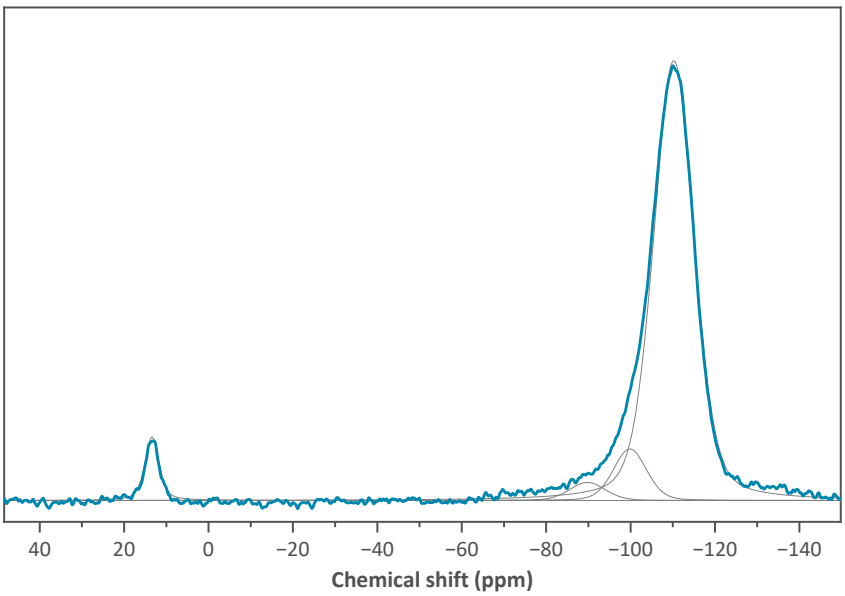

Figure 46. ^{29}Si Solid-state NMR of the TiO_2@SiO_2-tri-p4 catalyst

3.2 Catalytic tests

3.2.1 Optimization of titanium loading and passivation

After having evidenced the chemical and textural characteristics of a representative epoxidation catalyst based on trilobe-shaped silica pellets, we focused on the determination of the catalytic properties of this series of materials in the epoxidation of cyclohexene. The catalytic activity of TiO_2 supported on silica particles with different Si/Ti ratios (molar ratio from 0 to 153) was evaluated in the epoxidation reaction at 75°C. First, a 'blank' test was performed without any solid material (cf. Table 3~~Table 3~~, entry 1). As expected, the total amount of cyclohexene oxidation products was very low (less than 2% after 8 h) in the absence of a catalyst. Moreover, secondary products originating from the allylic oxidation of cyclohexene (cyclohexen-1-ol and cyclohexen-1-one) were detected in a similar proportion to the epoxide in this case. Then, the trimethylsilylated silica carrier SiO_2-tri-p was tested (cf. Table 3~~Table 3~~, entry 2). This material showed low catalytic activity in the formation of cyclohexene epoxide (2.8%). These results highlight the importance of the material passivation that promotes the epoxidation pathway compared to the allylic oxidation pathway.

The main part of this study concerns the investigation of the catalytic properties of titanium grafted trilobe-shaped pellets with variable Si/Ti ratios. To show the influence of the amount of the immobilized Ti on the catalytic activity, passivated silica trilobe-shaped supports with internal Si/Ti ratios ranging from 153 to 33 were tested as catalysts for the cyclohexene epoxidation reaction under identical experimental conditions (**Table 3**~~**Table 3**~~, entries 4, 5, 6, 7 and 8).

All the materials showed high catalytic activity and selectivity. Regarding the catalytic activities of the materials, a clear trend can be observed. As shown by the conversion of cumene hydroperoxide, the higher the amount of immobilized Ti, the higher the catalytic activity of the materials. For a Si/Ti ratio of 33 and a passivated material, complete conversion of cumene hydroperoxide was achieved within 8 h. Selectivity towards cyclohexene oxide (defined as the ratio of the epoxide yield to the sum of all cyclohexene oxidation product yields) was found to be above 90% for all the Ti-containing materials, with almost no side product detected with the TiO_2@SiO_2-tri-p4 catalyst.

Table 3. Effect of passivation and titanium-grafting on catalytic activity of silica pellet carriers for cyclohexene epoxidation (T = 75°C, m_{solid} = 0.1 g, V_L = 15.5 mL, $[cyclohexene]_0$ =5.4 M, $[cumene\ hydroperoxide]_0$ = 1.3 M, in presence of cumene, cumyl alcohol and toluene, fresh catalyst)

Entry	Catalyst	Residual amount of cyclohexene [(a),(b)] (%)	Cumene hydroperoxide conversion [(a),(c)] (%)	Yields of cyclohexene oxidation products [(a),(d)] (%)			
				Cyclohexene oxide	Cyclohexen-1-ol	Cyclohexen-1-one	Cyclohexane-1,2-diol
1	blank	89	n.q. [(f)]	0.4	1.0	0.2	n.d. [(f)]
2	SiO_2-tri-p	83	n.q. [(f)]	2.8	0.8	n.d.	n.d. [(f)]
3	TiO_2@SiO_2-tri-np1 [(e)]	72	71	18	0.4	n.d.	0.7
4	TiO_2@SiO_2-tri-p1	69	93	23	0.1	n.d.	0.2
5	TiO_2@SiO_2-tri-p2	72	96	21	0.5	0.2	1.1
6	TiO_2@SiO_2-tri-p3	67	89	21	0.3	n.d.	1.1
7	TiO_2@SiO_2-tri-p4	69	>99.9	25	0.1	n.d. [(f)]	n.d. [(f)]
8	TiO_2@SiO_2-tri-p5	69	>99.9	27	n.d.	n.d.	1.1

(a) after t = 8 h

(b) The residual amount of cyclohexene (CH) refers to $\frac{n_{CH(t)}}{n_{CH_0}}$ as the result of both the substrate oxidation and its removal from the reaction mixture by evaporation (where $n_{CH(t)}$ and n_{CH_0} are the number of moles of CH in the solution at time t and initial time of the reaction, respectively). Note also that in these experiments the olefin was in large excess with respect to the oxidant.

(c) The conversion of hydroperoxide (CHP) is calculated by $X_{CHP(t)} = \frac{n_{CHP_0} - n_{CHP(t)}}{n_{CHP_0}}$ (this reactant exhibiting low volatility).

(d) *cf.* equation (1)

(e) Si/Ti molar ratio = 121; np = non passivated

(f) n.d.: not detected; n.q.: not quantified (within the analysis uncertainty)

The significant effect of the trimethylsilanization on the catalytic properties of the support can also be inferred from the catalytic activities of the titanium-grafted silica carriers before and after passivation (TiO_2@SiO_2-tri-np1 and TiO_2@SiO_2-tri-p1, **Table 3**~~**Table 3**~~, entries 3/4). After passivation, the material exhibited a significantly higher catalytic activity in terms of hydroperoxide conversion (93% *vs*. 71%) and selectivity towards cyclohexene oxide (99% *vs*. 94%) than before trimethylsilylation of the surface. It resulted in lower amounts of cyclohexen-1-ol (from allylic oxidation) and cyclohexane-1,2-diol (from epoxide ring-opening). Such effects of the surface treatment on catalyst activity and selectivity were also reported by Silvestre-Alberó *et al.* for the cyclohexene epoxidation with tert-butylhydroperoxide on Ti-MCM-41 materials.[59]

Thus, the passivation step appears as an important aspect for the optimization of the catalytic properties of the materials, in particular for its selectivity.

In view of all these results, the TiO_2@SiO_2-tri-p4 catalyst with an internal Si/Ti ratio of 33 showed a good compromise between the amount of Ti involved for its synthesis and the catalytic performance for cyclohexene epoxidation (with total conversion of cumene hydroperoxide and epoxide selectivity of over 99%). This material has been chosen for further studies described below, in particular for the construction of a kinetic model. The stability and recyclability of this material were also assessed.

3.2.2 Metal loss and catalyst recycling

3.2.2.1 Catalytic activity of the leachate

We then focused on eventual leaching of the immobilized catalytic species and homogeneous contribution to the reaction. For this purpose, we carried out so-called ‘hot filtration tests’ in order to evaluate the catalytic activity of the leachate, after elimination of the heterogeneous catalyst by simple filtration. For this purpose, the reactant mixture was kept under heating for a further 6 h after removal of the TiO_2@SiO_2-tri-p4 catalyst at t = 2 h. It can clearly be seen that the epoxidation reaction did not further progress once the heterogeneous catalyst was removed (**Figure 5**~~**Figure 7**~~). This result shows that the catalytic activity of the leachate is negligible and that any significant homogeneous reaction contribution can be ruled out. Therefore, only a heterogeneous mechanism was considered for the epoxidation.

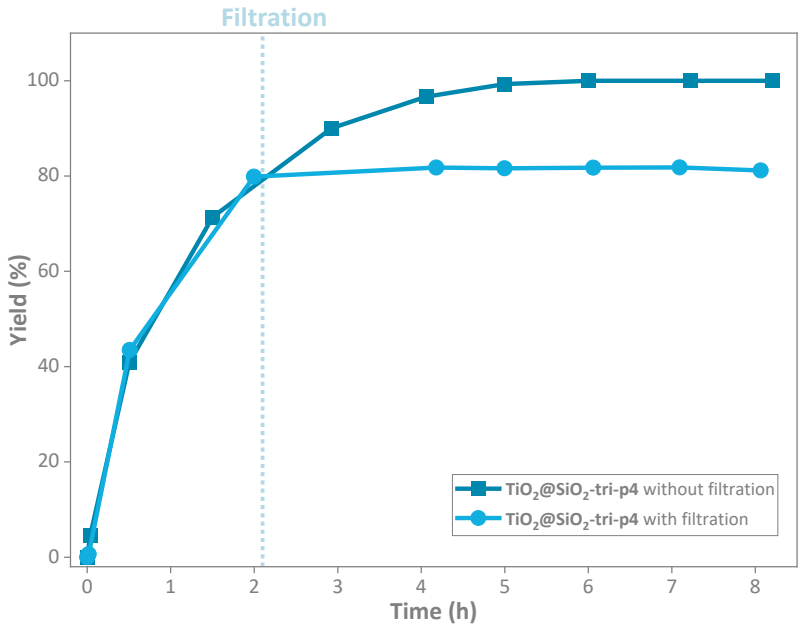

Figure 5~~7~~. Effect of catalyst removal after 2 h on the time-evolution of the cyclohexene oxide yield (T = 75°C, m_{cata} = 0.1 g, V_L = 15 mL, $[cyclohexene]_0$ = 5.2 M, $[cumene\ hydroperoxide]_0$ = 1.5 M, in the presence of cumene, cumyl alcohol and toluene, fresh catalyst)

3.2.2.2 Catalyst stability

The recyclability of the TiO_2@SiO_2-tri-p4 catalyst was assessed through multiple catalytic cycles of cyclohexene epoxidation using a single batch of this material. First, the reaction was performed at 75°C, in a 15 mL batch reactor, in the presence of toluene (in addition to cumene and cumyl alcohol from the cumene hydroperoxide solution). Prior to each reaction, the catalyst was washed with toluene, isopropanol, and acetone, and dried at 60°C under vacuum for 15 h. Our results show that the catalytic properties only slightly declined up to the fifth cycle, both in terms of catalytic activity and selectivity (**Figure 6~~Figure 8~~**). Whereas the CHP conversion decreased from 99.9% to 96.0% from the first to the fifth reaction cycle, the selectivity decreased from 99.6% to 98.8%. The catalyst reactivation process, which involves washing and low-pressure drying of the material, allowed for maintaining high catalytic performances for cyclohexene oxide formation during four reuse cycles. It also means that loss of titanium in solution should be negligible.

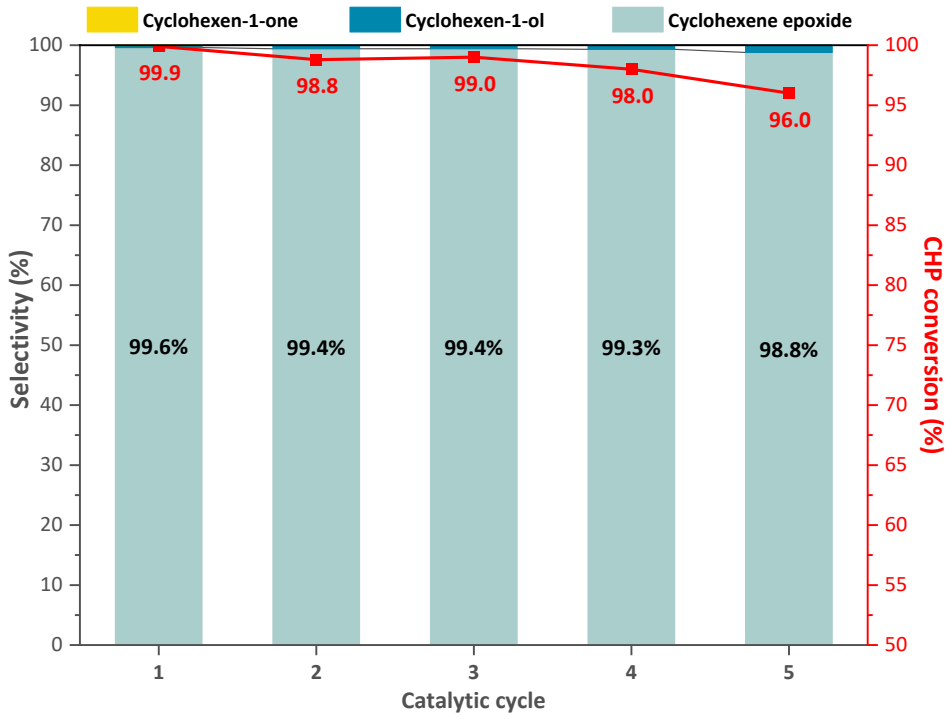

Figure 6~~8~~. Activity and selectivity of TiO_2@SiO_2-tri-p4 for cyclohexene epoxidation after several catalytic cycles (reaction time = 8 h, T = 75°C, m_{cata} = 0.1 g, V_L = 15 mL, $[cyclohexene]_0$ = 5.2 M, $[cumene\ hydroperoxide]_0$ = 1.5 M, in the presence of cumene, cumyl alcohol and toluene)

3.2.3 Kinetic study

3.2.3.1 Solvent effect

Following the preliminary tests carried out in the presence of toluene, the effect of replacing it by a less toxic solvent, namely cyclopentyl methyl ether (CPME), was thus evaluated. From their Kamlet-Taft (KT) parameters given in **Table 4~~Table 4~~**, it can be inferred that both solvents are aprotic (α = 0) and with a similar polarity (π^* = 0.4-0.5), but CPME has a significantly higher hydrogen bond basicity (β) and it is thus more coordinating. In addition, cumene, present together with the peroxide, exhibits KT parameters close to those of toluene.

In a coordinating solvent, the catalyst can form complexes with the solvent, thereby hindering the formation of the catalyst-hydroperoxide complex, and thus lowering the epoxidation rate.[60, 61]

Table 4. Kamlet-Taft parameters of toluene, cumene and CPME[62, 63]

Molecule	Polarity/polarizability (π^*)	Hydrogen-bond accepting ability or basicity (β)	Hydrogen-bond donating ability or acidity (α)
Toluene	0.50	0.12	0.00
Cumene	0.43	0.11	0.00
CPME	0.42	0.53	0.00

Each parameter is scaled between 0 and 1 with respect to two key reference solvents (*e.g.* π^*= 0 for cyclohexane and π^*= 1 for DMSO)

Following the preliminary recycling tests of the catalyst carried out in toluene, its deactivation was also investigated in CPME by recycling the pellets (within the basket) in the 150 mL reactor without any washing in between (**Erreur ! Source du renvoi introuvable.~~Figure 9~~**). A decrease in the initial epoxidation rate is observed between the first and second catalyst use which might be ascribed to some "conditioning" of the catalyst (*e.g.*, removal of solvents or extra silanization agent used during the catalyst preparation). Catalyst activity is further reduced in subsequent recycles, which might be due to products and/or solvent remaining adsorbed on the active sites at the expense of the reactants, as shown in section 3.2.3.2. Therefore, the reaction rates measured during the very first reuses of the catalyst (second and third uses of the catalyst giving the same results) were expected to be more relevant for the kinetic study with a view to catalyst utilization in a continuous flow reactor.

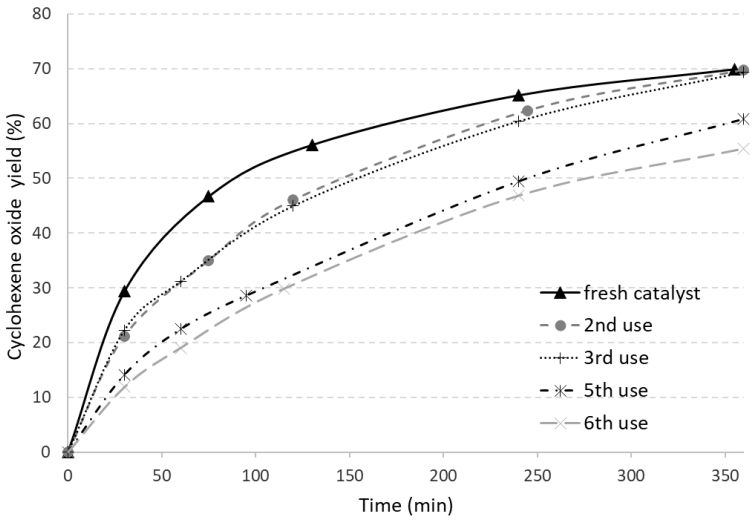

Figure ~~7~~9. Effect of catalyst recycling on the time-evolution of cyclohexene oxide yield (T = 80°C, m_{cat} = 1 g, V_L = 75 mL, [cyclohexene]$_0$ = 1.8 M, [cumene hydroperoxide]$_0$ = 1.8 M, CPME as solvent)

From **Figure 8**~~**Figure 10**~~, which compares the time-concentration profiles of the reactants and epoxide product in the two solvents, it can be concluded that the epoxidation performance obtained in CPME and toluene is actually essentially the same: the difference in the concentration profiles is in the order of magnitude of the experimental deviation of 4% measured by triplicating the reaction test in reference conditions. Moreover, the amount of epoxide formed during the reaction matches that of hydroperoxide consumed, suggesting that ring-opening of the epoxide moiety can be neglected. The slightly higher apparent conversion of cyclohexene might be due to substrate evaporation, resulting in some condensate loss on the reactor lid. Indeed, the amount of oxidation by-products (2-cyclohexen-1-ol and 2-cyclohexen-1-one) does not exceed 1.5% of the total products. Therefore, only the cyclohexene oxide yield will be shown in the following graphs.

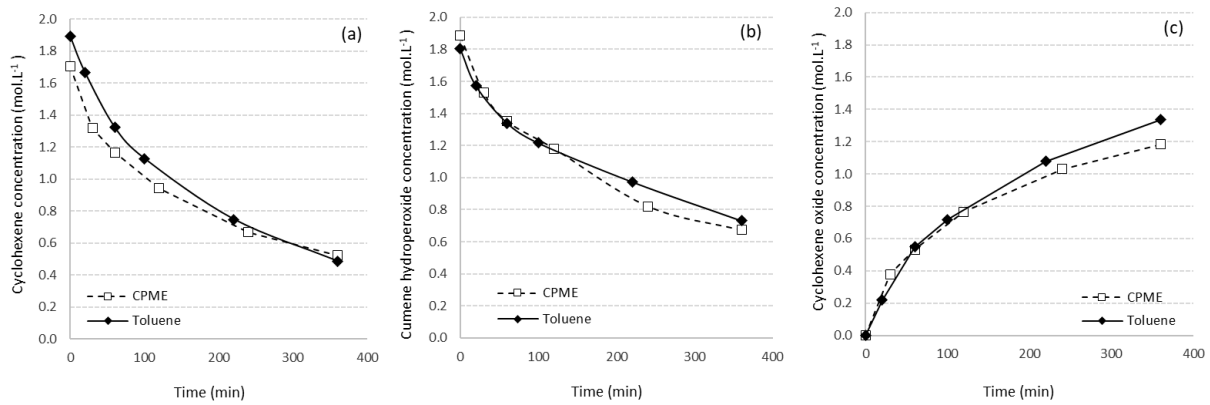

Figure 8~~**10**~~**.** Effect of the solvent (CPME *vs.* toluene) on the time-concentration profiles of cyclohexene (a), cumene hydroperoxide (b) and cyclohexene oxide (c) (T = 80°C, m_{cat} = 1 g, V_L = 75 mL, $[cyclohexene]_0$ = 1.8 M, $[cumene\ hydroperoxide]_0$ = 1.8 M, 3rd catalyst use)

Furthermore, the effect of diluting the reactants with the solvent was investigated by varying the initial concentrations of the olefin and the oxidant to the same extent (ca. 3 M concentration of the reactants being achieved without CPME). Epoxidation kinetics are reported to exhibit a positive order with respect to both cyclohexene and peroxide.[64-68] Therefore, starting from a stoichiometric reactant mixture, a decrease in the substrate conversion, and thus in the epoxidation yield, can be expected at lower reactant concentrations due to dilution effect (apart from a possible interaction of the solvent with the catalyst). On the other hand, rate inhibition

by product adsorption (epoxide and/or alcohol) is also mentioned,[65, 66, 68, 69] where increasing the amount of solvent should have a positive effect. In addition, cumene hydroperoxide is much more viscous than CPME, resulting in lower species diffusivities and a higher mass transfer resistance by diffusion within the porous catalyst.

Figure 9~~Figure 11~~ reveals that the reactant dilution should have a greater impact, as increasing the solvent amount appears to reduce the epoxidation yield.

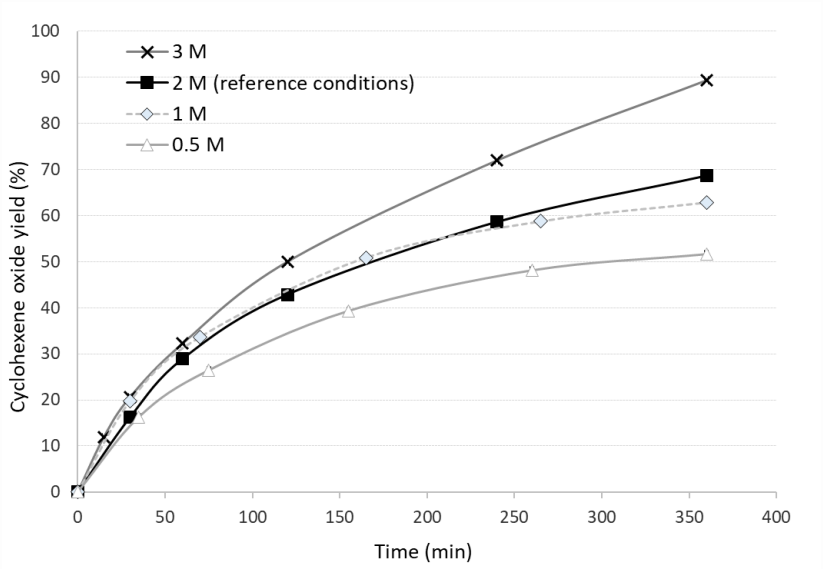

Figure 9~~11~~. Effect of diluting the reactants (in stoichiometric amounts) on the time-evolution of cyclohexene oxide yield (T = 80°C, m_{cat} = 1 g, V_L = 75 mL, $[cyclohexene]_0$ = $[cumene\ hydroperoxide]_0$ = 0.5-3.2 M, CPME as solvent, 2nd catalyst use)

3.2.3.2 Product inhibition

To quantify the effect of product inhibition, the solution obtained after the reaction was completed with the same amount of cyclohexene and cumene hydroperoxide as the starting solution to be recycled for a subsequent reaction. Figure 10~~Figure 12~~ confirms that the presence of reaction products induces a significant decrease in the initial epoxidation rate, by about a factor of 3, with the cyclohexene oxide yield after 6 h decreasing from 69% to 53%. Introducing separately the sole epoxide and cumyl alcohol into the starting solution resulted into a similar effect. There is thus a competition for the active sites between the reactants and the two products.

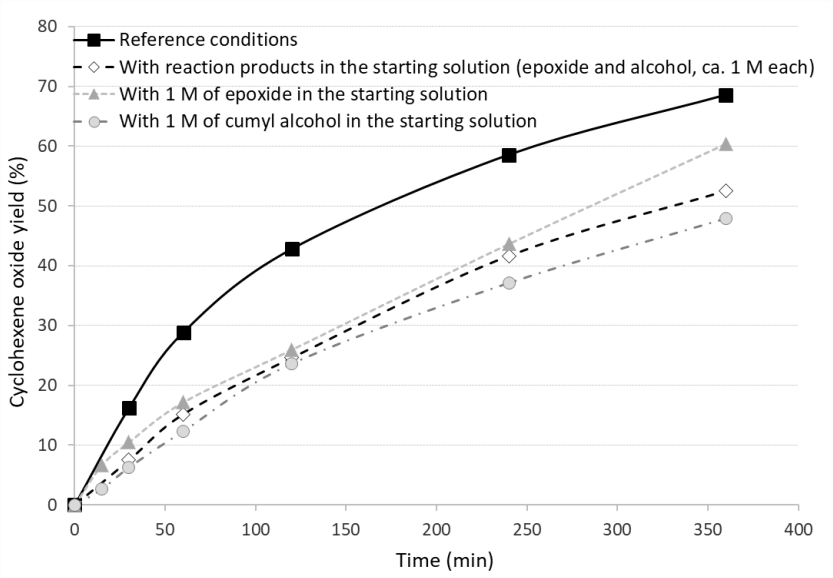

Figure 10~~12~~. Effect of product inhibition on the time-evolution of cyclohexene oxide yield (T = 80°C, m_{cat} = 1 g, V_L = 75-100 mL, $[cyclohexene]_0$ = 1.4-1.8 M, $[cumene\ hydroperoxide]_0$ = 1.4 -1.8 M, CPME as solvent, 2nd and 3rd catalyst use)

3.2.3.3 Influence of oxidant to substrate ratio

A positive effect of increasing the oxidant excess with respect to the substrate can be deduced from **Figure 11~~Figure 13~~**, either for a given substrate concentration (**Figure 11~~Figure 13~~a**) or for a given oxidant concentration (**Figure 11~~Figure 13~~b**), although less pronounced in the latter case. These results indicate a positive reaction order with respect to cumene hydroperoxide, and a fractional reaction order for cyclohexene, since a higher epoxide yield relative to the substrate is found when the oxidant concentration is increased or the substrate concentration is decreased. Logarithm plots of the corresponding initial rates indeed give apparent reaction orders with respect to cumene hydroperoxide and cyclohexene of 0.50 and 0.76, respectively. These values are of the same order as those given by Wu et al. for the epoxidation of propylene by H_2O_2 over a supported TS-1 catalyst: 0.32 for the oxidant and 0.68 for the substrate.[67]

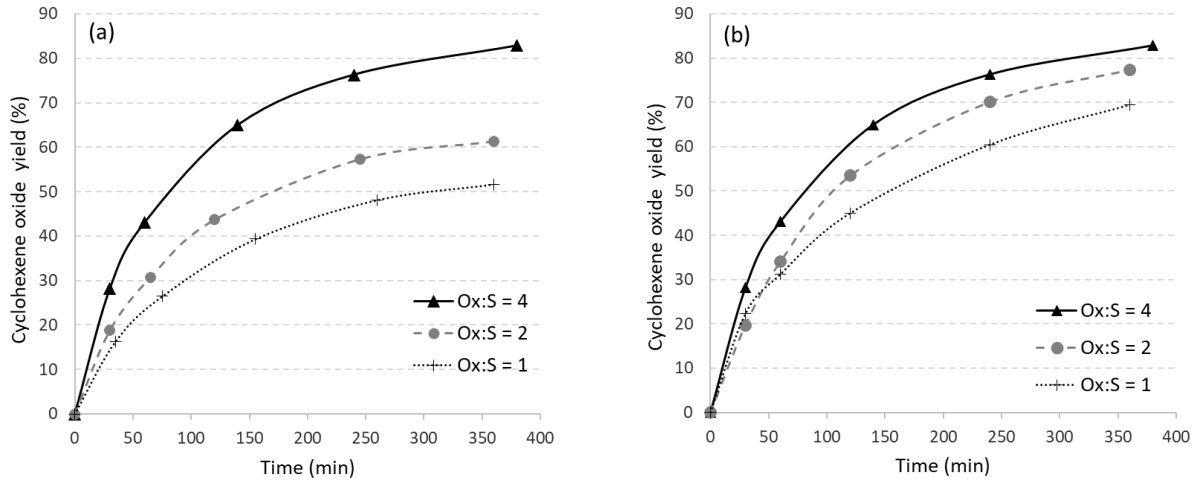

Figure 11~~13~~. Effect of the oxidant to substrate ratio (Ox:S) on the time-evolution of cyclohexene oxide yield for $[cyclohexene]_0$ = 0.5 M (a) and for $[cumene\ hydroperoxide]_0$ = 1.9 M (b) (T = 80°C, m_{cat} = 1 g, V_L = 75 mL, CPME as solvent, 2nd catalyst use)

3.2.3.4 Apparent activation energy

A significant effect of the temperature on the epoxide yield is observed in **Figure 12~~Figure 14~~**. The Arrhenius plot of the initial rates gives an apparent activation energy of 27.2 kJ.mol^{-1}. However, this value is lower than those reported in the literature for the epoxidation of C2-C4 olefins over Ti-based catalysts, which range between 40 and 52 kJ.mol^{-1}.[36, 64, 67, 70] With the exception of Wu et al. ,[67] the above mentioned authors used powder catalysts, which suggests the occurrence of diffusion limitations within the TiO_2@SiO_2-tri-p4 millimeter-sized pellets.

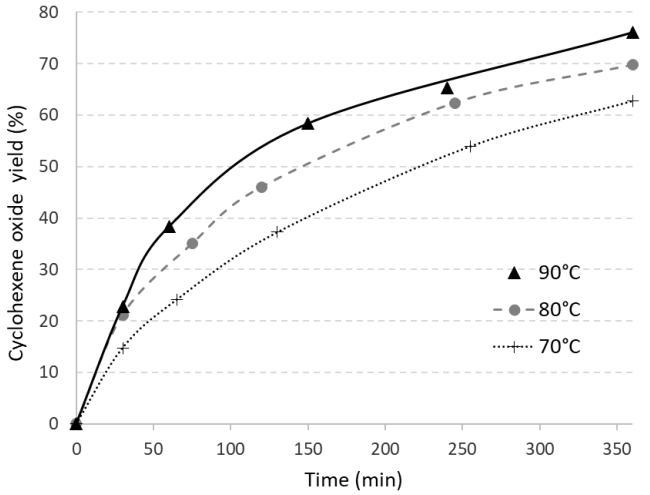

Figure 12~~14~~. Effect of temperature on the time-evolution of cyclohexene oxide yield (T = 80°C, m_{cata} = 1 g, V_L = 75-100 mL, $[cyclohexene]_0$ = 1.8 M, $[cumene\ hydroperoxide]_0$ = 1.8 M, CPME as solvent, 2nd catalyst use)

3.2.3.5 Evaluation of internal diffusion limitations

The Weisz modulus compares the observed rate of consumption of a reactant to its effective diffusion rate in the porous catalytic material. A value less than 0.1 indicates that the overall reaction rate is controlled by the intrinsic reaction rate (chemical reaction-limited regime), while a value above 3 refers to a strong limitation by internal diffusion (diffusion-limited regime).[71-73]

The Weisz moduli $\phi'_{s0,i}$ of the reactants were evaluated at time t = 0 in the reference conditions (80°C, stoichiometric reactant solution at 2 M each) from the following equation:

$$\phi'_{s0,i} = \left(\frac{n+1}{2}\right) \cdot \frac{r_{app0,i} \cdot L^2}{D_{e,i} \cdot C_{s0,i}} \qquad (2)$$

where $D_{e,i}$ (in $m^3_L . m^{-1}_{cata} . s^{-1}$) is the effective diffusivity of the reactant i in the porous catalyst ($D_{e,i} = \frac{\varepsilon_p \cdot D_{m,i}}{\tau_p}$ for liquid-phase species with ε_p the porosity of the catalyst, τ_p its tortuosity factor and $D_{m,i}$ the molecular diffusion of the reactant in the liquid), $C_{i,s0}$ is the initial concentration of the reactant ($mol.m^{-3}_L$) at the catalyst surface (assumed equal to its concentration in the liquid bulk in the absence of external diffusion limitation), $r_{app0,i}$ is its initial apparent reaction rate (here taken equal to the initial epoxidation rate, in $mol.m^{-3}_{cata}.s^{-1}$), L is the catalyst diffusion length (ratio of the catalyst volume to its external surface area, in m_{cata})and n is the reaction order.

The molecular diffusivities of cyclohexene and cumene hydroperoxide were estimated at $5.1 \cdot 10^{-9}$ and $6.8 \cdot 10^{-9}$ $m^2.s^{-1}$, respectively, according to the Wilke-Chang equation.[74] The TiO_2@SiO_2-tri-p4 trilobe extrudate has a L value of 0.32 mm (since titanium is homogeneously distributed up to the core of the particle) and a porosity ε_p ($V_{pores}/V_{trilobe}$) of 0.63 (see §3.1). Using a typical value of 5 for the tortuosity factor τ_p and n values between 1 and 2 (diffusion of both the reactants in a stoichiometric amount being limiting), Equation (2) results in a value of the Weisz modulus between 1.5 and 2.2 based on cumene hydroperoxide diffusivity. Under these conditions, the reaction using the trilobe catalyst is thus significantly limited by internal pore diffusion (it should operate in the end of intermediate to beginning of diffusional regime).

This limitation is confirmed by comparing the time-evolution of the epoxide yield for the TiO_2@SiO_2-tri-p4 pellets and the corresponding powdered catalyst with d_{43} (volume-weighted

mean diameter) equal to 80 µm (for which $\phi'_{s0,i} \leq 0.1$), Figure 13~~Figure 15~~. Indeed, the ratio of the initial rates of the two catalysts gives an effectiveness factor of ca. 0.3.

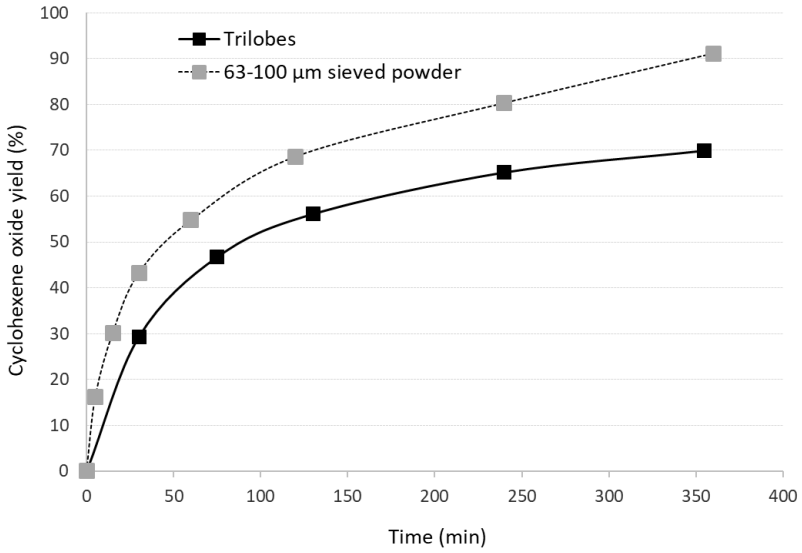

Figure 13~~15~~. Comparison of the time-evolution of the evolution of cyclohexene oxide yield for the trilobed and the powdered catalyst (T = 80°C m_{cat} = 1 g, V_L = 75 mL, $[cyclohexene]_0$ = 1.8 M, $[cumene\ hydroperoxide]_0$ = 1.8 M, CPME as solvent, fresh catalyst, d_{43} = 80 µm for the powdered catalyst)

3.2.4 Kinetic model

Based on the experimental data measured in the 150 mL reactor, an apparent reaction rate model was fitted using Matlab 2022 software to describe the epoxidation kinetics in CPME with the TiO_2@SiO_2-tri-p4 catalyst. It is recalled that in this case the oxidant was used in a stoichiometric or excess amount, in order to allow quantitative conversion of the olefin.

3.2.4.1 Epoxidation rate expression

According to the literature,[67, 69] alkene epoxidation usually obeys an Eley-Rideal type (E-R) mechanism, in which the free alkene (here cyclohexene, CH) directly reacts with the adsorbed peroxide (cumene hydroperoxide, CHP). Such a reaction involves the elementary steps described by Equations (3) to (7), including reversible adsorption/desorption steps and an irreversible surface reaction:

$$CH + * \rightleftarrows CH* \qquad \text{Fast (eq. cst } K_{CH}) \qquad (3)$$

$$CHP + * \rightleftarrows CHP* \qquad \text{Fast (eq. cst } K_{CH}) \qquad (4)$$

$$CHP* + CH \longrightarrow CHO + COH + * \qquad \text{RDS (rate cst k)} \qquad (5)$$

$$CHO + * \rightleftarrows CHO* \qquad \text{Fast (eq. cst } K_P) \qquad (6)$$

$$COH + * \rightleftarrows COH* \qquad \text{Fast (eq. cst } K_O) \qquad (7)$$

where * stands for the free titanium sites and X* for the adsorbed species X. This reaction scheme considers the possible adsorption of the alkene on the active sites, as well as that of the epoxide (cyclohexene oxide, CHO) and the produced alcohol (cumyl alcohol, COH). It should be noted that the initial concentration of COH in the reactant mixture was about 10% that of the peroxide. Assuming that the surface reaction is the rate-determining step, the overall epoxidation rate can then be expressed according to Equation (8):

$$r_{E\text{-}R} = \frac{k_{E\text{-}R} \cdot K_{CHP} \cdot [CHP] \cdot [CH]}{1 + K_{CH} \cdot [CH] + K_{CHP} \cdot [CHP] + K_{CHO} \cdot [CHO] + K_{COH} \cdot [COH]} \qquad (8)$$

with the concentrations [X] expressed in $mol.L^{-1}$ and $r_{E\text{-}R}$ in $mol.g_{cata}^{-1}.s^{-1}$.

The reaction rate constant $k_{E\text{-}R}$ (in $L.g_{cata}^{-1}.s^{-1}$) and the adsorption equilibrium constants K_X (in $L.mol^{-1}$) depend upon temperature, according to the Arrhenius law (Equation (9)) and the Van't Hoff equation, respectively.

$$k_{E\text{-}R}(T) = k_{E\text{-}R,0} \cdot exp\left(\frac{-E_A}{R_g \cdot T}\right) \qquad (9)$$

where $k_{E\text{-}R,0}$ is the pre-exponential constant of the E-R rate equation ($L.g_{cata}^{-1}.s^{-1}$), E_A is the activation energy ($J.mol^{-1}$), R_g the universal gas constant (8.314 $J.mol^{-1}.K^{-1}$), and T the actual temperature (K).

Although the resistance to internal diffusion could not be ignored for the pellet catalyst as demonstrated in §3.2.3.5, the same rate expression as given by Equation (8) was also used to model the apparent kinetics. To reduce the number of parameters in the optimisation, the variation of the adsorption equilibrium constants with temperature was ignored, considering the relatively narrow temperature range. Furthermore, since the synthesized Ti-SiO_2 catalyst was found to be highly selective for the cyclohexene epoxidation, only this reaction was considered for the species mass balances. We further simplified the E-R model by neglecting cyclohexene adsorption (as detailed in Equation (10)) since its reaction order was close to 1. Additionally, we evaluated the relevance of the Langmuir–Hinshelwood (L-H) mechanism, with a reaction between adsorbed CHP and adsorbed CH (Equation (11)).

$$r_{E\text{-}Rs} = \frac{k_{E\text{-}Rs} \cdot K_{CHP} \cdot [CHP] \cdot [CH]}{1 + K_{CHP} \cdot [CHP] + K_{CHO} \cdot [CHO] + K_{COH} \cdot [COH]} \qquad (10)$$

$$r_{L\text{-}H} = \frac{k_{L\text{-}H} \cdot K_{CH} \cdot K_{CHP} \cdot [CHP] \cdot [CH]}{(1 + K_{CH} \cdot [CH] + K_{CHP} \cdot [CHP] + K_{CHO} \cdot [CHO] + K_{COH} \cdot [COH])^2} \qquad (11)$$

3.2.4.2 Optimization procedure

Time-dependent mass balances, consisting in a system of ordinary differential equations, were solved using the Matlab function 'ode15s', with a variable-step variable-order solver based on the numerical differentiation formulas of orders 1 to 5.[75] For the optimization of the kinetic parameters, the sum of squared errors (SSE) between the theoretical and experimental concentrations of the epoxide was selected as the objective function to be minimized (Equation (11)).

$$SSE = f(p) = \sum_{j=1}^{m} \sum_{i=1}^{n(j)} \left(\mathrm{C_{CHO,theo}}_{i,j}(p) - \mathrm{C_{CHO,exp}}_{i,j} \right)^2 \quad (11)$$

where m is the number of considered experiments, $n(j)$ is the number of data points in the experiment j and p is the set of kinetic parameters.

The Arrhenius law equation (Equation (9)) was reparametrized according to Equation (12) to reduce the correlation between the pre-exponential factor and the activation energy.[76]

$$k(T) = k_{T_{ref}} \cdot exp\left(\frac{-E_A}{R_g} \left(\frac{1}{T} - \frac{1}{T_{ref}} \right) \right) \quad (12)$$

where $k_{T_{ref}}$ is the reaction rate constant at T_{ref}, chosen within the investigated temperature range (here T_{ref} = 353.15 K).

A hybrid optimization approach was applied to fit a dataset comprising 14 experiments (with 5 data points each) conducted at variable temperatures (60°C-90°C) and variable initial concentrations of the reactants (0.5 M-2 M) to pinpoint the minimum of the objective function. The Matlab optimization script involved a sequential utilization of the 'fmincon' function (a gradient-based algorithm for constrained nonlinear optimization)[77] followed by a simulated annealing ('simulannealbnd') algorithm (global stochastic method). The lower bound of the kinetic parameters was set to zero.

In order to evaluate the model performance, we calculated the coefficient of determination, R^2 as described in Equation (13):

$$R^2 = 1 - \frac{SSE}{SST} \quad (13)$$

where SST is the total sum of squares between the epoxide concentrations measured and their overall mean $\overline{C}_{\mathrm{CHO,exp}}$ defined in Equation (14):

$$SST = \sum_{j=1}^{m} \sum_{i=1}^{n(j)} \left(C_{\mathrm{CHO,exp}_{i,j}} - \overline{C}_{\mathrm{CHO,exp}} \right)^2 \quad (14)$$

3.2.4.3 Model results

Table 5~~Table 5~~ gives the parameters and the coefficient of determination of the three kinetic models studied. The Eley-Rideal model (R^2 = 0.984) better fits the experimental data with respect to the Langmuir-Hinshelwood model (R^2 = 0.946), in agreement with previous results in the literature.[67, 70] Optimization of the original Eley-Rideal model leads to a very small value for the adsorption constant of cyclohexene K_{CH}, so that its contribution collapses in the denominator sum. Therefore, the simplified E-R model, which neglects its effect, represents the experimental data equally well, indicating a near first order with respect to the substrate. The values of the adsorption constants of the products reveal a stronger inhibition by the epoxide, but this result should be qualified by the fact that the selected database does not include experiments in which the reaction products were intentionally introduced in the starting mixture (cumyl alcohol being found in the peroxide solution, in a molar ratio of about 1:10). For the three models, the apparent activation energy is of the order of 24 kJ.mol^{-1}, which is close to the estimate given in §3.2.3.4.

Table 5. Parameters of the investigated reaction rate models

Model	k_0	E_A [c]	K_{CH} [d]	K_{CHP} [d]	K_{CHO} [d]	K_{COH} [d]	R^2
E-R	0.11 [a]	24.3	$6.7 \cdot 10^{-5}$	0.31	0.86	0.29	0.983
simplified E-R	0.11 [a]	24.3	-	0.32	0.86	0.28	0.984
L-H	0.29 [b]	24.3	0.99	1.05	1.00	0.68	0.946

[a] Unit of pre-exponential constant for E-R model: $L \cdot g_{cata}^{-1} \cdot s^{-1}$
[b] Unit of pre-exponential constant for L-H model: $mol \cdot g_{cata}^{-1} \cdot s^{-1}$
[c] Unit of apparent activation energy: $kJ.mol^{-1}$
[d] Unit of adsorption constants: $L \cdot mol^{-1}$

The time-evolution of the epoxide yield, predicted by the optimized simplified E-R model, is compared with the experimental data in Figure 14~~Figure 16~~ for the 14 conditions. Overall, the calculated yields are in fairly good agreement with the experimental results.

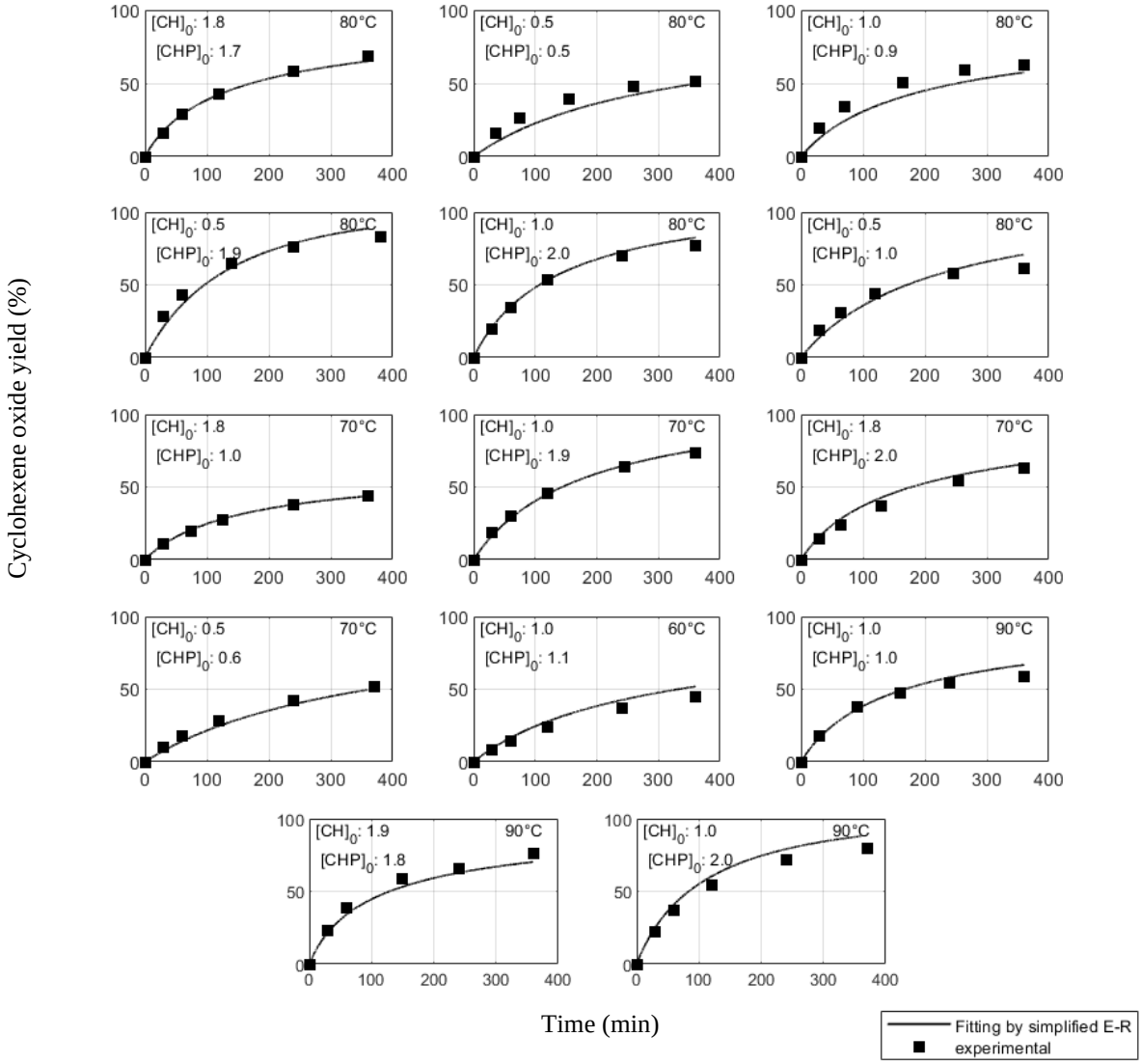

initial concentrations $[X]_0$ in $mol.L^{-1}$

Figure 14~~16~~. Comparison between experimental data and model predictions of the time-evolution of cyclohexene oxide yield (T = 60°C-80°C, m_{cata} = 1 g, V_L = 75 mL, $[cyclohexene]_0$ = 0.5-2 M, $[cumene\ hydroperoxide]_0$ = 0.5-2 M, CPME as solvent, 2nd and 3rd catalyst uses)

4 Conclusion

We report a novel heterogeneous epoxidation catalyst based on trilobed-shaped silica pellets. The material was obtained by a two-step sequence involving titanium grafting via impregnation/calcination, followed by surface passivation via trimethylsilylation. A series of materials with variable Si/Ti ratios could easily be achieved via addition of variable amounts of the molecular titanium(IV) isopropoxide to the impregnation solution. The resulting materials were thoroughly characterized in order to determine their chemical composition together with their textural properties. In particular, the SEM/EDX analyses showed that a catalyst with Ti content up to 2 wt.%, homogeneously distributed across the pellet cross-section, could be achieved, without significantly reducing the porosity of the silica carrier. Moreover, XPS spectroscopy revealed that the grafted titanium was mainly inserted in a tetrahedral coordination. Catalytic tests in epoxidation reactions of cyclohexene revealed excellent catalytic properties in terms of catalytic activity and selectivity. In particular, a material displaying a Si/Ti molar ratio of 33 exhibited promising catalytic properties, which remained stable over several consecutive reuse cycles in both toluene and a greener solvent alternative, cyclopentyl methyl ether (CPME). Therefore, it was selected for a detailed kinetic study carried out in CPME. In the investigated conditions with stoichiometric or excess amount of the oxidant, the reaction rate could be fitted by an Eley-Rideal model including adsorption of the oxidant and inhibition by the formed products (as evidenced by recycling the solution or introducing the products in the initial reactant mixture), while the adsorption of the substrate could be neglected. Limitations due to internal diffusion of the reactants in the porous structure of the trilobed-shape pellets were evidenced, resulting in an apparent activation energy of 24.3 $kJ.mol^{-1}$, lower than reported in the previous studies.

Overall, we have shown that trilobed-shaped silica pellets are a suitable support for the elaboration of heterogeneous epoxidation catalysts. This finding is of particular importance for process scale-up as it will allow the application in a fixed bed type reactor. Based on the developed kinetic model, ongoing work addresses the translation of batch to continuous conditions using a catalytic heat-exchanger reactor.

Acknowledgements

This work was part of the CATASIC project, funded by the French National Research Agency under the grant ANR-20-CE08-0029. The authors also wish to thank Maïko Riodel, Lahcen

Farhi (ST LGC) and Alec Manoury (CRITT GPTE, Toulouse) for the assembly of the 150 mL stirred reactor set-up, Marie-Line de Solan, Christine Rey-Rouch, Gwenaëlle Guittier (SAP LGC), Diane Samelor and Jérôme Esvan (CIRIMAT, Toulouse) for their help on the characterizations of the materials by SEM/EDX, morphology analysis (pellets) and laser diffraction (powder), mercury intrusion porosimetry, UV-Vis and XPS spectroscopy, respectively, Anaïs Vandenbossche (SAP LGC) for her support on the GC analyses of the samples, Gregory Ribeiro (LGC) for his work on the kinetic optimization.

Supporting Information

This information is available free of charge via the Internet at http://pubs.acs.org/.

References

(1) Tsuji, J.; Yamamoto, J.; Ishino, M.; Oku, N. Development of New Propylene Oxide Process. *Sumitomo Kagaku* **2006**, *2006-1* (1), 1.
(2) Zakkour, P.; Cook, G. *CCS Roadmap for Industry: High-purity CO2 sources*; Carbon Counts, 2010. https://downloads.unido.org/ot/47/85/4785083/ENVIRONMENT_High%20Purity_FINAL%20DRAFT.pdf.
(3) Meng, Y. D.; Taddeo, F.; Aguilera, A. F.; Cai, X. S.; Russo, V.; Tolvanen, P.; Leveneur, S. The Lord of the Chemical Rings: Catalytic Synthesis of Important Industrial Epoxide Compounds. *Catalysts* **2021**, *11* (7), 765. DOI: 10.3390/catal11070765.
(4) Penn, L. S.; Chiao, T. T. Epoxy Resins. In *Handbook of Composites*, Lubin, G. Ed.; Vol. 1; Springer, 1982.
(5) Schneberger, G. L. *Adhesives in Manufacturing*; Taylor & Francis, 1983. DOI: 10.1201/9781315136691.
(6) Van Ogtrop, J.; Smaardijk, A. A.; Stichter, H. Processes for the production of ethylene glycol. United States of America 2012.
(7) Akindoyo, J. O.; Beg, M. D. H.; Ghazali, S.; Islam, M. R.; Jeyaratnam, N.; Yuvaraj, A. R. Polyurethane types, synthesis and applications - a review. *RSC Advances* **2016**, *6* (115), 114453-114482. DOI: 10.1039/c6ra14525f.
(8) Kothandaraman, J.; Heldebrant, D. J. Catalytic coproduction of methanol and glycol in one pot from epoxide, CO_2, and H_2. *RSC Advances* **2020**, *10* (69), 42557-42563. DOI: 10.1039/d0ra09459e.
(9) Allen, S. D.; Moore, D. R.; Lobkovsky, E. B.; Coates, G. W. High-activity, single-site catalysts for the alternating copolymerization of CO_2 and propylene oxide. *Journal of the American Chemical Society* **2002**, *124* (48), 14284-14285. DOI: 10.1021/ja028071g.
(10) Alves, M.; Grignard, B.; Mereau, R.; Jerome, C.; Tassaing, T.; Detrembleur, C. Organocatalyzed coupling of carbon dioxide with epoxides for the synthesis of cyclic

carbonates: catalyst design and mechanistic studies. *Catalysis Science & Technology* **2017**, *7* (13), 2651-2684. DOI: 10.1039/c7cy00438a.
(11) de la Torre, O.; Renz, M.; Corma, A. Biomass to chemicals: Rearrangement of β-pinene epoxide into myrtanal with well-defined single-site substituted molecular sieves as reusable solid Lewis-acid catalysts. *Applied Catalysis a-General* **2010**, *380* (1-2), 165-171. DOI: 10.1016/j.apcata.2010.03.056.
(12) Omonov, T. S.; Curtis, J. M. Plant Oil-Based Epoxy Intermediates for Polymers. In *Bio-Based Plant Oil Polymers and Composites*, Madbouly, S. A., Zhang, C., Kessler, M. R. Eds.; Elsevier, 2016; pp 99-125.
(13) Brandolese, A.; Kleij, A. W. Catalyst Engineering Empowers the Creation of Biomass-Derived Polyesters and Polycarbonates. *Accounts of Chemical Research* **2022**, *55* (12), 1634-1645. DOI: 10.1021/acs.accounts.2c00204.
(14) de Oliveira, M. P.; Delolo, F. G.; Villarreal, J. A. A.; dos Santos, E. N.; Gusevskaya, E. V. Hydroformylation and one-pot hydroformylation/epoxy ring cleavage of limonene oxide: A sustainable access to biomass-based multi-functional fragrances. *Applied Catalysis a-General* **2021**, *616*, 118082. DOI: 10.1016/j.apcata.2021.118082.
(15) Monterde, M. I.; Lombard, M.; Archelas, A.; Cronin, A.; Arand, M.; Furstoss, R. Enzymatic transformations.: Part 58:: Enantioconvergent biohydrolysis of styrene oxide derivatives catalysed by the *Solanum tuberosum* epoxide hydrolase. *Tetrahedron-Asymmetry* **2004**, *15* (18), 2801-2805. DOI: 10.1016/j.tetasy.2004.06.032.
(16) Bedore, M. W.; Zaborenko, N.; Jensen, K. F.; Jamison, T. F. Aminolysis of Epoxides in a Microreactor System: A Continuous Flow Approach to β-Amino Alcohols. *Organic Process Research & Development* **2010**, *14* (2), 432-440. DOI: 10.1021/op9003136.
(17) Kim, J.; Hayashi, Y.; Badr, S.; Okamoto, K.; Hakogi, T.; Furukawa, H.; Yoshikawa, S.; Nakanishi, H.; Sugiyama, H. Hybrid Modeling of an Active Pharmaceutical Ingredient Flow Synthesis in a Ring-Opening Reaction of an Epoxide with a Grignard Reagent. *Industrial & Engineering Chemistry Research* **2023**, *62* (43), 17824-17834. DOI: 10.1021/acs.iecr.3c02137.
(18) Thomas, R. M.; Widger, P. C. B.; Ahmed, S. M.; Jeske, R. C.; Hirahata, W.; Lobkovsky, E. B.; Coates, G. W. Enantioselective Epoxide Polymerization Using a Bimetallic Cobalt Catalyst. *Journal of the American Chemical Society* **2010**, *132* (46), 16520-16525. DOI: 10.1021/ja1058422.
(19) Brocas, A. L.; Mantzaridis, C.; Tunc, D.; Carlotti, S. Polyether synthesis: From activated or metal-free anionic ring-opening polymerization of epoxides to functionalization. *Progress in Polymer Science* **2013**, *38* (6), 845-873. DOI: 10.1016/j.progpolymsci.2012.09.007.
(20) Longo, J. M.; Sanford, M. J.; Coates, G. W. Ring-Opening Copolymerization of Epoxides and Cyclic Anhydrides with Discrete Metal Complexes: Structure-Property Relationships. *Chemical Reviews* **2016**, *116* (24), 15167-15197. DOI: 10.1021/acs.chemrev.6b00553.
(21) Suo, H. Y.; Liu, S.; Liu, J. Y.; Zhang, Z. S.; Qu, R.; Gu, Y. A.; Qin, Y. S. Novel epoxide-promoted polymerization of lactides mediated by a zinc guanidine complex: a potential strategy for the tin-free PLA industry. *Polymer Chemistry* **2023**, *14* (40), 4652-4658. DOI: 10.1039/d3py00890h.
(22) Nijhuis, T. A.; Makkee, M.; Moulijn, J. A.; Weckhuysen, B. M. The production of propene oxide: Catalytic processes and recent developments. *Industrial & Engineering Chemistry Research* **2006**, *45* (10), 3447-3459. DOI: 10.1021/ie0513090.
(23) Sienel, G.; Rieth, R.; Rowbottom, K. T. Epoxides. In *Ullmann's Encyclopedia of Industrial Chemistry*, Wiley-VCH Verlag GmbH & Co. KGaA, 2000.
(24) Grigoropoulou, G.; Clark, J. H.; Elings, J. A. Recent developments on the epoxidation of alkenes using hydrogen peroxide as an oxidant. *Green Chemistry* **2003**, *5* (1), 1-7. DOI: 10.1039/b208925b.

(25) Dai, P. E.; Lunsford, J. H. Catalytic Properties of molybdenum zeolites in epoxidation reactions. 2. Oxidation of cyclohexene. *Journal of Catalysis* **1980**, *64* (1), 184-199. DOI: 10.1016/0021-9517(80)90491-1.
(26) El-Korso, S.; Khaldi, I.; Bedrane, S.; Choukchou-Braham, A.; Thibault-Starzyk, F.; Bachir, R. Liquid phase cyclohexene oxidation over vanadia based catalysts with tert-butyl hydroperoxide: Epoxidation versus allylic oxidation. *Journal of Molecular Catalysis a-Chemical* **2014**, *394*, 89-96. DOI: 10.1016/j.molcata.2014.07.002.
(27) Lin, Y. C.; Chang, C. C.; Sung, K. H.; Lee, J. F.; Cheng, S. Importance of solvents in preparing highly active Ti-SBA-15 catalysts by grafting method. *Microporous and Mesoporous Materials* **2018**, *272*, 276-285. DOI: 10.1016/j.micromeso.2018.06.046.
(28) Wulff, H. P.; Wattimena, F. Olefin Epoxidation. United States of America 1972.
(29) Clerici, M. G.; Bellussi, G.; Romano, U. Synthesis of propylene-oxide from propylene and hydrogene peroxide catalyzed by titanium silicalite. *Journal of Catalysis* **1991**, *129* (1), 159-167. DOI: 10.1016/0021-9517(91)90019-z.
(30) Notari, B. Titanium silicalites. *Catalysis Today* **1993**, *18* (2), 163-172. DOI: 10.1016/0920-5861(93)85029-y.
(31) Schmidt, F.; Bernhard, M.; Morell, H.; Pascaly, M. HPPO Process Technology A novel route to propylene oxide without coproducts. *Chimica Oggi-Chemistry Today* **2014**, *32* (2), 31-35.
(32) Russo, V.; Tesser, R.; Santacesaria, E.; Di Serio, M. Chemical and Technical Aspects of Propene Oxide Production via Hydrogen Peroxide (HPPO Process). *Industrial & Engineering Chemistry Research* **2013**, *52* (3), 1168-1178. DOI: 10.1021/ie3023862.
(33) Chiker, F.; Launay, F.; Nogier, J. P.; Bonardet, J. L. Green and selective epoxidation of alkenes catalysed by new TiO_2-SiO_2 SBA mesoporous solids. *Green Chemistry* **2003**, *5* (3), 318-322. DOI: 10.1039/b300244f.
(34) Dong, P.; Shao, T. N.; Li, J. L.; Zhang, X. H.; Zhao, Y.; Zhao, X. H.; Li, G. X. An Overview of Heterogeneous Transition Metal-Based Catalysts for Cyclohexene Epoxidation Reaction. *European Journal of Inorganic Chemistry* **2023**, e202300483. DOI: 10.1002/ejic.202300483.
(35) Shilcrat, S. Process Safety Evaluation of a Tungsten-Catalyzed Hydrogen Peroxide Epoxidation Resulting In a Runaway Laboratory Reaction. *Organic Process Research & Development* **2011**, *15* (6), 1464-1469. DOI: 10.1021/op200133q.
(36) Alvear, M.; Orabona, F.; Eränen, K.; Lehtonen, J.; Rautiainen, S.; Di Serio, M.; Russo, V.; Salmi, T. Epoxidation of light olefin mixtures with hydrogen peroxide on TS-1 in a laboratory-scale trickle bed reactor: Transient experimental study and mathematical modelling. *Chemical Engineering Science* **2023**, *269*, 118467. DOI: 10.1016/j.ces.2023.118467.
(37) Kamegawa, T.; Yamahana, D.; Seto, H.; Yamashita, H. Preparation of single-site Ti-containing mesoporous silica with a nanotube architecture and its enhanced catalytic activities. *Journal of Materials Chemistry A* **2013**, *1* (3), 891-897. DOI: 10.1039/c2ta00331g.
(38) Wróblewska, A.; Malko, M.; Walasek, M. Environmental friendly method of the epoxidation of limonene with hydrogen peroxide over the Ti-SBA-15 catalyst. *Polish Journal of Chemical Technology* **2018**, *20* (4), 6-12. DOI: 10.2478/pjct-2018-0047.
(39) Esipovich, A. L.; Belousov, A. S.; Kanakov, E. A.; Mironova, V. Y.; Rogozhin, A. E.; Danov, S. M.; Vorotyntsev, A. V.; Makarov, D. A. Solvent Effects in Epoxidation of Fatty Acid Methyl Esters with Hydrogen Peroxide over TS-1 Catalyst. *Kinetics and Catalysis* **2019**, *60* (1), 62-68. DOI: 10.1134/s0023158419010063.
(40) He, Z. W.; Lei, Q. F.; Dai, W. L.; Zhang, H. B. Solvent tunes the selectivity of alkenes epoxidation over Ti-Beta Zeolite: A systematic kinetic assessment on elementary steps, kinetically relevant and reaction barriers. *Journal of Catalysis* **2023**, *421*, 172-184. DOI: 10.1016/j.jcat.2023.03.012.

(41) de Gonzalo, G.; Alcántara, A. R.; de María, P. D. Cyclopentyl Methyl Ether (CPME): A Versatile Eco-Friendly Solvent for Applications in Biotechnology and Biorefineries. *ChemSusChem* **2019**, *12* (10), 2083-2097. DOI: 10.1002/cssc.201900079.
(42) Azzena, U.; Carraro, M.; Pisano, L.; Monticelli, S.; Bartolotta, R.; Pace, V. Cyclopentyl Methyl Ether: An Elective Ecofriendly Ethereal Solvent in Classical and Modern Organic Chemistry. *ChemSusChem* **2019**, *12* (1), 40-70. DOI: 10.1002/cssc.201801768.
(43) Hutter, R.; Mallat, T.; Baiker, A. Titania-silica mixed oxides. 2. Catalytic behavior in olefin epoxidation. *Journal of Catalysis* **1995**, *153* (1), 177-189. DOI: 10.1006/jcat.1995.1119.
(44) Coles, M. P.; Lugmair, C. G.; Terry, K. W.; Tilley, T. D. Titania-silica materials from the molecular precursor Ti $[OSi(O^tBu)_3]_4$: Selective epoxidation catalysts. *Chemistry of Materials* **2000**, *12* (1), 122-131. DOI: 10.1021/cm990444y.
(45) Capel-Sanchez, M. C.; Blanco-Brieva, G.; Campos-Martin, J. M.; de Frutos, M. P.; Wen, W.; Rodriguez, J. A.; Fierro, J. L. G. Grafting Strategy to Develop Single Site Titanium on an Amorphous Silica Surface. *Langmuir* **2009**, *25* (12), 7148-7155. DOI: 10.1021/la900578u.
(46) Capel-Sanchez, M. C.; Barrio, L.; Campos-Martin, J. M.; Fierro, J. L. G. Silylation and surface properties of chemically grafted hydrophobic silica. *Journal of Colloid and Interface Science* **2004**, *277* (1), 146-153. DOI: 10.1016/j.jcis.2004.04.055.
(47) Smeets, V.; Gaigneaux, E. M.; Debecker, D. P. Titanosilicate Epoxidation Catalysts: A Review of Challenges and Opportunities. *ChemCatChem* **2022**, *14* (1), e202101132. DOI: 10.1002/cctc.202101132.
(48) Rouquerol, J.; Baron, G.; Denoyel, R.; Giesche, H.; Groen, J.; Klobes, P.; Levitz, P.; Neimark, A. V.; Rigby, S.; Skudas, R.; et al. Liquid intrusion and alternative methods for the characterization of macroporous materials (IUPAC Technical Report). *Pure and Applied Chemistry* **2012**, *84* (1), 107-136. DOI: 10.1351/pac-rep-10-11-19.
(49) Khouchaf, L.; Boulahya, K.; Das, P. P.; Nicolopoulos, S.; Kis, V. K.; Lábár, J. L. Study of the Microstructure of Amorphous Silica Nanostructures Using High-Resolution Electron Microscopy, Electron Energy Loss Spectroscopy, X-ray Powder Diffraction, and Electron Pair Distribution Function. *Materials* **2020**, *13* (19), 4393. DOI: 10.3390/ma13194393.
(50) Adhikary, S. K.; Rudzionis, Z.; Tuckute, S.; Ashish, D. K. Effects of carbon nanotubes on expanded glass and silica aerogel based lightweight concrete. *Scientific Reports* **2021**, *11* (1), 2104. DOI: 10.1038/s41598-021-81665-y.
(51) Aigner, M.; Grosso-Giordano, N. A.; Okrut, A.; Zones, S.; Katz, A. Epoxidation of 1-octene under harsh tail-end conditions in a flow reactor I: a comparative study of crystalline vs. amorphous catalysts. *Reaction Chemistry & Engineering* **2017**, *2* (6), 842-851. DOI: 10.1039/c7re00076f.
(52) Andresen, M.; Johansson, L. S.; Tanem, B. S.; Stenius, P. Properties and characterization of hydrophobized microfibrillated cellulose. *Cellulose* **2006**, *13* (6), 665-677. DOI: 10.1007/s10570-006-9072-1.
(53) Zhang, X.; Zhang, F.; Chan, K. Y. Synthesis of titania-silica mixed oxide mesoporous materials, characterization and photocatalytic properties. *Applied Catalysis a-General* **2005**, *284* (1-2), 193-198. DOI: 10.1016/j.apcata.2005.01.037.
(54) Sulym, I.; Goncharuk, O.; Sternik, D.; Skwarek, E.; Derylo-Marczewska, A.; Janusz, W.; Gun'ko, V. M. Silica-Supported Titania-Zirconia Nanocomposites: Structural and Morphological Characteristics in Different Media. *Nanoscale Research Letters* **2016**, *11*, 111. DOI: 10.1186/s11671-016-1304-1.
(55) Chaowamalee, S.; Yan, N.; Ngamcharussrivichai, C. Propylsulfonic Acid-Functionalized Mesostructured Natural Rubber/Silica Nanocomposites as Promising Hydrophobic Solid Catalysts for Alkyl Levulinate Synthesis. *Nanomaterials* **2022**, *12* (4), 604. DOI: 10.3390/nano12040604.

(56) Ferreira-Neto, E. P.; Ullah, S.; Martinez, V. P.; Yabarrena, J.; Simoes, M. B.; Perissinotto, A. P.; Wender, H.; de Vicente, F. S.; Noeske, P. L. M.; Ribeiro, S. J. L.; Rodrigues, U. P. Thermally stable SiO_2@TiO_2 core@shell nanoparticles for application in photocatalytic self-cleaning ceramic tiles. *Materials Advances* **2021**, *2* (6), 2085-2096. DOI: 10.1039/d0ma00785d.
(57) Guo, W. Z.; Kortenbach, T.; Qi, W.; Hensen, E.; Heeres, H. J.; Yue, J. Selective tandem catalysis for the synthesis of 5-hydroxymethylfurfural from glucose over in-situ phosphated titania catalysts: Insights into structure, bi-functionality and performance in flow microreactors. *Applied Catalysis B-Environmental* **2022**, *301*, 120800. DOI: 10.1016/j.apcatb.2021.120800.
(58) Massiot, D.; Fayon, F.; Capron, M.; King, I.; Le Calvé, S.; Alonso, B.; Durand, J. O.; Bujoli, B.; Gan, Z. H.; Hoatson, G. Modelling one- and two-dimensional solid-state NMR spectra. *Magnetic Resonance in Chemistry* **2002**, *40* (1), 70-76. DOI: 10.1002/mrc.984.
(59) Silvestre-Alberó, J.; Domine, M. E.; Jordá, J. L.; Navarro, M. T.; Rey, F.; Rodríguez-Reinoso, F.; Corma, A. Spectroscopic, calorimetric, and catalytic evidences of hydrophobicity on Ti-MCM-41 silylated materials for olefin epoxidations. *Applied Catalysis a-General* **2015**, *507*, 14-25. DOI: 10.1016/j.apcata.2015.09.029.
(60) Sheldon, R. A.; Vandoorn, J. A.; Schram, C. W. A.; Dejong, A. J. Metal-catalyzed epoxidation of olefins with organic hydroperoxides: II. The effect of solvent and hydroperoxide structure. *Journal of Catalysis* **1973**, *31* (3), 438-443. DOI: 10.1016/0021-9517(73)90315-1.
(61) Mirzaee, M.; Bahramian, B.; Gholizadeh, J.; Feizi, A.; Gholami, R. Acetylacetonate complexes of vanadium and molybdenum supported on functionalized boehmite nano-particles for the catalytic epoxidation of alkenes. *Chemical Engineering Journal* **2017**, *308*, 160-168. DOI: 10.1016/j.cej.2016.09.055.
(62) Jessop, P. G.; Jessop, D. A.; Fu, D. B.; Phan, L. Solvatochromic parameters for solvents of interest in green chemistry. *Green Chemistry* **2012**, *14* (5), 1245-1259. DOI: 10.1039/c2gc16670d.
(63) Sherwood, J. R. Bio-Based Solvents for Organic Synthesis. PhD Thesis, University of York, 2013.
(64) Li, K. T.; Lin, P. H.; Lin, S. W. Preparation of Ti/SiO_2 catalysts by chemical vapor deposition method for olefin epoxidation with cumene hydroperoxide. *Applied Catalysis a-General* **2006**, *301* (1), 59-65. DOI: 10.1016/j.apcata.2005.11.012.
(65) Ruddy, D. A.; Tilley, T. D. Kinetics and mechanism of olefin epoxidation with aqueous H_2O_2 and a highly selective surface-modified TaSBA15 heterogeneous catalyst. *Journal of the American Chemical Society* **2008**, *130* (33), 11088-11096. DOI: 10.1021/ja8027313.
(66) Shin, S. B.; Chadwick, D. Kinetics of Heterogeneous Catalytic Epoxidation of Propene with Hydrogen Peroxide over Titanium Silicalite (TS-1). *Industrial & Engineering Chemistry Research* **2010**, *49* (17), 8125-8134. DOI: 10.1021/ie100083u.
(67) Wu, G. Q.; Wang, Y. Q.; Wang, L. N.; Feng, W. P.; Shi, H. N.; Lin, Y.; Zhang, T.; Jin, X.; Wang, S. H.; Wu, X. X.; Yao, P. X. Epoxidation of propylene with H_2O_2 catalyzed by supported TS-1 catalyst in a fixed-bed reactor: Experiments and kinetics. *Chemical Engineering Journal* **2013**, *215*, 306-314. DOI: 10.1016/j.cej.2012.11.055.
(68) Ardagh, M. A.; Bregante, D. T.; Flaherty, D. W.; Notestein, J. M. Controlled Deposition of Silica on Titania-Silica to Alter the Active Site Surroundings on Epoxidation Catalysts. *ACS Catalysis* **2020**, *10* (21), 13008-13018. DOI: 10.1021/acscatal.0c02937.
(69) Morlanes, N.; Notestein, J. M. Kinetic study of cyclooctene epoxidation with aqueous hydrogen peroxide over silica-supported calixarene-Ta(V). *Applied Catalysis a-General* **2010**, *387* (1-2), 45-54. DOI: 10.1016/j.apcata.2010.07.063.
(70) Liang, X. H.; Mi, Z. T.; Wu, Y. L.; Wang, L.; Xing, E. H. Kinetics of epoxidation of propylene over TS-1 in isopropanol. *Reaction Kinetics and Catalysis Letters* **2003**, *80* (2), 207-215. DOI: 10.1023/B:REAC.0000006127.34574.a7.

(71) Levenspiel, O. Chapter 18: Solid Catalyzed Reactions. In *Chemical Reaction Engineering Third Edition*, John Wiley & Sons, 1999; pp 376-426.
(72) De Wilde, J.; Froment, G. F.; Bischoff, K. B. Chapter 3: Transport Processes with Reactions Catalyzed by Solids. In *Chemical Reactor Analysis and Design*, John Wiley & Sons, 2010.
(73) Fogler, H. S. Chapter 15: Diffusion and Reaction. In *Elements of Chemical Reaction Engineering, Fifth Edition*, Prentice Hall, 2016; pp 719-766.
(74) Wilke, C. R.; Chang, P. Correlation of diffusion coefficients in dilute solutions. *Aiche Journal* **1955**, *1* (2), 264-270. DOI: 10.1002/aic.690010222.
(75) Shampine, L. F.; Gladwell, I.; Thompson, S. *Solving ODEs with MATLAB*; Cambridge University Press, 2003.
(76) Schwaab, M.; Lemos, L. P.; Pinto, J. C. Optimum reference temperature for reparameterization of the Arrhenius equation. Part 2: Problems involving multiple reparameterizations. *Chemical Engineering Science* **2008**, *63* (11), 2895-2906. DOI: 10.1016/j.ces.2008.03.010.
(77) Byrd, R. H.; Gilbert, J. C.; Nocedal, J. A trust region method based on interior point techniques for nonlinear programming. *Mathematical Programming* **2000**, *89* (1), 149-185. DOI: 10.1007/pl00011391.